Yeast double transporter-gene deletion library for identification of xenobiotic carriers in low or high throughput

Ludimila Dias Almeida[a], Ali Salim Faraj Silva[a], Daniel Calixto Mota[a], Adrielle Ayumi Vasconcelos[b], Antônio Pedro Camargo[b], Gabriel Silva Pires[a], Monique Furlan[a], Helena Martins Ribeiro da Cunha Freire[a], Angélica Hollunder Klippel[c], Suélen Fernandes Silva[d], Cleslei Fernando Zanelli[c], Marcelo Falsarella Carazzolle[b], Stephen G. Oliver[e]# & Elizabeth Bilsland [a,e]#

[a] Synthetic Biology Laboratory, Department of Structural and Functional Biology, Institute of Biology, University of Campinas—UNICAMP, Campinas, São Paulo, Brazil

[b] Laboratory of Genomics and BioEnergy, Department of Genetics, Evolution, Microbiology and Immunology, Institute of Biology, University of Campinas—UNICAMP, Campinas, São Paulo, Brazil

[c] School of Pharmaceutical Sciences, São Paulo State University—UNESP, Araraquara, São Paulo, Brazil

[d] Chemistry Institute, São Paulo State University—UNESP, Araraquara, São Paulo, Brazil

[e] Cambridge Systems Biology Centre & Department of Biochemistry, University of Cambridge, Cambridge, United Kingdom

Running Head:

Yeast library for the identification of xenobiotic import routes.

Corresponding authors:

Elizabeth Bilsland: bilsland@unicamp.br

Stephen G. Oliver: sgo24@cam.ac.uk

Abstract and importance word count: 241

Text word count: 5,391

Abstract

The routes of uptake and efflux should be considered when developing new drugs so that they can effectively address their intracellular targets. As a general rule, drugs appear to enter cells via protein carriers that normally carry nutrients or metabolites. A previously developed pipeline that searched for drug transporters using *Saccharomyces cerevisiae* mutants carrying single-gene deletions identified import routes for most compounds tested. However, due to the redundancy of transporter functions, we propose that this methodology can be improved by utilizing double-mutant strains in both low- and high-throughput screens. We constructed a library of over 14,000 strains harboring double-deletions of genes encoding 122 non-essential plasma membrane transporters, and performed low- and high-throughput screens identifying possible drug import routes for 23 compounds. In addition, the high-throughput assay enabled the identification of putative efflux routes for 21 compounds. Focusing on azole antifungals, we were able to identify the involvement of the *myo*-inositol transporter, Itr1p, in the uptake of these molecules and to confirm the role of Pdr5p in their export.

Importance

Our library of double transporter deletion strains is a powerful tool for rapid identification of potential drug import and export routes, which can aid in determining the chemical groups necessary for transport via specific carriers. This information may be translated into a better design of drugs for optimal absorption by target tissues and

the development of drugs whose utility is less likely to be compromised by the selection of resistant mutants.

Keywords

Saccharomyces cerevisiae; non-essential transporter double-deletion library; plasma membrane transporter; drug uptake; drug efflux; xenobiotics

Introduction

Novel drug candidates are generally designed based on the assumption that they enter cells by passive diffusion through the plasma membrane lipid bilayer. Thus, compounds that do not follow the rules predicting an efficient diffusion through the lipid bilayer are not considered drug-like and are discarded early in the drug discovery process. However, a growing body of evidence indicates that passive diffusion via the lipid bilayer is an exceptional, rather than the normal, mode of drug entry (1–6) with most drugs (and other xenobiotics) entering cells via protein carriers that normally carry nutrients or metabolites.

The investigation of the carrier substrate specificity is one of the objectives of the RESOLUTE consortium, a public-private partnership that aims to study the therapeutic potential of the human solute carrier (SLCs) proteins superfamily (7). This consortium works to create tools for studying these proteins on a large scale to associate specific classes of compounds with particular carriers. Therefore, knockout and tagged overexpression cell libraries are being built for most SLCs to carry out the 'guilt-by-association' strategy. By using these approaches, the RESOLUTE consortium seeks to contribute to the inclusion of this superfamily of carriers in the class of classic drug targets.

Given the importance of mapping drug-transporter interactions to enabling a rational targeting of drugs to the tissues of interest, a method was developed to screen for yeast

transmembrane proteins that mediated drug absorption; this identified the import routes for half of the screened anticancer compounds (8). The strategy assumes that a drug is toxic when present inside the cell in high concentration; thus, if the yeast does not have the carrier protein responsible for the entry of that molecule, it becomes drug resistant and survives (Figure 1). Strains with deletions of individual genes encoding each of the non-essential transporters of the *Saccharomyces cerevisiae* plasma membrane were employed for transporter identification (8). The same approach was also used to study the specificity of human solute carriers on the import of 60 cytotoxic compounds using an SLC-specific CRISPR – Cas9 knockout (KO) library, suggesting the association between SLCs and the transport of 47 out of 60 compounds (~ 80%) (9), a proportion similar to that observed in the yeast study (18/26; ~ 70%) (8). In addition, CRISPR – Cas9 was also employed for large-scale transporter disruption in *S. cerevisiae* strains, aiming at the identification of carrier-mediated routes (10).

Yeast deletion libraries have been widely used, in genomic chemical-profiling strategies, to study cellular responses to both new molecules and established drugs (11). In this approach, libraries with heterozygous deletions of all genes (haploinsufficiency profiling - HIP) or homozygous non-essential genes (homozygous deletion profiling - HOP) are employed in genetic screens to evaluate the cellular response to these molecules. Extensive studies have tested large numbers of molecules (12, 13) using these approaches and the data are available to the research community. Based on the strategy previously presented for the identification of xenobiotic transporters, HOP data for

strains with deletions of membrane transporters can provide insights into possible routes of entry for the screened molecules. However, the experimental design employed in most HOP assays aims to identify strains sensitive to low concentrations of test compounds and is not directly comparable to screens utilizing toxic concentrations (as required for transporter identification assays). Furthermore, proteins and drugs are highly promiscuous, with many drugs interacting with multiple off-target proteins in most cells (14). This promiscuity is not exclusive to the intracellular targets of drugs, but also occurs in the trans-membrane import and export of drug compounds (15).

Due to the redundancy of transport functions between transmembrane proteins, we concluded that a larger set of drug import routes could be identified by testing drug import activity in strains lacking pairs of transporters. Hence, to screen for epistatic interactions between genes encoding transporter proteins, we constructed a library of *S. cerevisiae* strains containing double-deletion mutations of all pairwise combinations of genes that specify non-essential transmembrane transporters. We have characterized the performance of this double-mutant collection in drug screening, employing both low- and high-throughput strategies (Figure 2). These studies have reinforced our initial hypothesis that most drugs enter cells preferentially through plasma membrane transporters.

Results

Double-deletion library construction

The library with 14,640 strains carrying double deletions of genes encoding non-essential membrane transporters was built utilizing the Synthetic Genetic Arrays (SGA) methodology. Genetic crosses were performed between a strain carrying a deletion due to replacement of a transporter gene with the *kan*MX cassette flanked by up- and down-stream barcodes for tracking deletions and a second transporter deletant containing the *nat*MX replacement cassette, but without the barcodes. Non-essential gene deletants were selected (from the library of strains available in the laboratory) based on their transporter function and plasma membrane expression (16).

Commercial xenobiotics cytotoxic to yeast

To allow a further characterization of our transporter double-deletion library, and determine plasma membrane import routes for different xenobiotic compounds, we purchased 32 compounds that largely obey the Lipinski's "rule of 5" (17) and are therefore expected to be preferentially imported into the cells by passive diffusion through the lipid bilayer (Table S1). The carrier-mediated import route of 13 of these compounds had been evaluated previously (8), using a single-transporter gene-deletion library. However, this earlier study was not able to define the specific transporter for all the tested compounds, perhaps due to carrier promiscuity.

We determined an approximate IC_{90} for each compound's effect on yeast in liquid cultures and proceeded to select for resistance in plates with sub-lethal doses of each compound. We performed serial dilutions of wild type (BY4741), the transporter double-mutant, and single-mutant pools and spotted these onto YNB+Sc agar plates with inhibitory concentrations of the commercial xenobiotics (Figure 3). Single-gene deletion mutants for genes encoding cytoplasmic non-transporter proteins were included (*trx2*Δ::kanMX and *cpr1*Δ::kanMX) as controls. The xenobiotics for which we did not observe significant growth inhibition at 200 µM (maximum of 2% DMSO; 400 µM for artesunate and 800 µM for dl-4-hydroxy-3-methoxymandelic acid and tamoxifen) in solid media were excluded from further screens (Figure 3).

Using spot assays, we defined which compounds were toxic to yeast in solid media and the appropriate concentration to inhibit the growth of the wild type strain whilst selecting for resistant strains from the library pool. For some compounds, we were able to observe a clear difference in resistance between wild type and the transporter deletants, as shown in Figure 3. In addition, we were able to identify compound-inhibitory differences between double- and single-deletant libraries. It is expected, for a compound imported by a transporter, that the double-deletion library will present double the number of resistant strains than the single-deletion library, even when only one transporter is involved in the uptake. We saw this pattern on using inhibitory concentrations of 1,2,4-triazoles (epoxiconazole, difenoconazole, and tebuconazole) and chlorothalonil, for example (Figure 3). Thus, working with a double-deletion library can

facilitate the identification of transporters. However, in several cases we observed more colonies in the single-deletion library that could be due to differences in strain background, as a number of different markers were introduced in the double mutant strains to allow large-scale selection of the desired haploids.

We employed two approaches for compound transporter identification: a low- and a high-throughput strategy. The low-throughout method is a plate-based screen with the selection of resistant strains in the presence of inhibitory concentrations of xenobiotics and identification of transporter deletions bearing the *kan*MX cassette by barcode sequencing. This strategy allows a visual assessment of a possible involvement of transporters in drug uptake and the identification of candidate import routes. The second approach was the high-throughput screening, where we evaluated the fluctuation of abundance of transporter-deletion strains by sequencing the *kan*MX upstream barcodes from the library pool in a liquid culture containing inhibitory concentrations of a compound. This screening allowed us to identify not only strains resistant to a given compound, but also strains sensitive to this compound.

Low-throughput (plate-based) strategy for xenobiotic transporter identification

Xenobiotic-resistant strains from the transporter double-deletion library pool were selected by plating 10^6, 10^5, 10^4 and 10^3 colony-forming units (CFUs) of wild type BY4741 or the transporter-deletion pool onto YNB+Sc agar plates containing inhibitory concentrations of the compounds (Figure 4 and data not shown). We expected to

observe an even growth inhibition of the wild type strain and the appearance of resistant colonies (corresponding to the deletion of genes encoding transporters responsible for drug uptake) on plates where the compounds enter cells through plasma membrane transporters. For the selection of xenobiotic-resistant strains from the library pool, we investigated the difference between the number of resistant colonies, aiming to define conditions in which more deletant colonies could grow on the pool plate in comparison to that of the wild type. However, we also observed cases in which the greatest differences between wild type and transporter deletion pools were the formation of colonies with different sizes, hence we collected the largest colonies to identify the deleted carrier gene. This was the case for 5-fluorocytosine and fluconazole, for example (Figure 4). Once 20-40 resistant colonies were selected for each xenobiotic, barcodes (associated with *kan*MX cassette) from approximately 20 strains were sequenced to identify the transporter-genes that had been deleted.

After aligning the sequenced barcodes to the *Saccharomyces* Genome Deletion Project's barcode list (18), we identified the genes deleted in each compound-resistant strain (Table 1). It is important to note that, as only the genes deleted with *kan*MX were barcoded, the sequencing results only show one of the transporter-encoding genes deleted in the compound-resistant strain. Furthermore, as during the library construction we had several copies of the *his3* deletion in all mating plates, this deletion is present in high frequency in the library. Hence, *HIS3* "hits" were excluded from further data analysis. As expected, for 5-fluorocytosine, the positive control of the study, 7 out

of 10 of the carriers identified by deletion with the *kan*MX cassette correspond to Fcy2p (gene *FCY2* - YER056C). For the other three 5-fluorocytosine resistant strains selected, the deletion of *FCY2* was identified by PCR with the *nat*MX cassette (data not shown).

Analyzing the results in plate assays (Table 1), we could observe recurrent transporter-gene deletions for some compounds. This is best exemplified by the ketoconazole results, where 14 resistant strains were *nha1*Δ. Other compounds showed preferential representation of certain transporter-gene deletion strains, indicating their potential involvement in compound import. Although these results suggested possible transporters, additional assays are needed to confirm these phenotypes. In fact, plate-screening assays can give rise to false positives, requiring a larger sample size to confirm the hits. Thus, for a more comprehensive screening, with the monitoring of the fluctuation in the abundance of all strains in the pool, we performed a high-throughput assay in liquid culture.

High-throughput (liquid-growth) strategy for xenobiotic transporter identification

The putative import and export routes of xenobiotic compounds were investigated by Chemical Genomic Profiling (CGP) using our double-mutant non-essential transporter-gene deletion library. The library was cultivated in liquid cultures containing inhibitory concentrations of xenobiotics for ca. 15 generations and the *kan*MX upstream barcodes from the population were sequenced for transporter-gene deletion identification. Thus, we were able to identify deletions responsible for resistance (putative import route) and

sensitivity (putative export route) to the test compounds (Figure 5, Table 1, Data set S1). Treatment with 5-fluorocytosine identified the *fcy2*Δ mutant as the most abundant strain of the assay, confirming the accuracy of the method.

Among the significantly less abundant strains (padj ≤ 0.1; p-value ≤ 0.001; $\log_2$ fold change ≤ 0.5), we could identify deletions for genes encoding ATP-binding cassette (ABC) drug efflux pumps involved in pleiotropic drug resistance: Pdr5p, Snq2p and Yor1p (19) (Data set S1). The *pdr5*Δ mutation caused sensitivity to artesunate, irgasan, iprobenfos, and azoles; the latter being consistent with published results (20, 21). The *snq2*Δ mutation caused sensitivity to artesunate, carbendazim, and chlorothalonil. The *yor1*Δ mutation caused sensitivity only to tunicamycin. Pdr11p, a PDR family member involved in sterol uptake (22), was identified among mutations that conferred sensitivity to artesunate, captan, chlorothalonil, difenoconazole, N-phenylanthranilic acid, tamoxifen, and tunicamycin. The PDR11 paralog, AUS1, involved in sterol uptake (22), was not represented among depleted strains. We also identified Nft1p, a putative transporter of the MRP subfamily (23), as a candidate exporter for epoxiconazole, tebuconazole, difenoconazole, and 5-fluorocytosine.

Multi-drug resistance transporters can also belong to the Major Facilitator Superfamily (MFS) (24, 25); however, these had little impact on sensitivity to our test compounds, with the following exceptions: *flr1*Δ (chlorothalonil and 3,4-dicloroisocoumarin), *dtr1*Δ (fluconazole), *qdr1*Δ (5-fluorocytosine), *qdr2*Δ (5-fluorocytosine), and *atr1*Δ (5-

fluorocytosine). It should be noted that some transporters of this class (e.g. Flr1p) have been reported to be determinants of resistance to compounds tested in this study (e.g. fluconazole) (26), however, our CGP did not confirm these correlations.

Principal components analysis (PCA) allows an evaluation of the distribution of variations between replicates and conditions within an experiment. Figure 6 and Figure S1 show that the strain composition in the pool following some treatments is very similar to the control (DMSO) in both the first and second principal components. It is important to note that replicates of each xenobiotic cluster within the same region of the PCA plot, and that the azoles tested (with the exception of fluconazole) present very similar strain composition profiles, which validates the reproducibility of the experiments. We would also note that 5-fluorocytosine (Figure S1) shows a very different profile when compared to all other treatments in the analysis, with the exception of fluconazole (Figure 6).

Overview of putative import routes for the xenobiotics

Some of the compounds evaluated in our assays were not cytotoxic in either liquid or solid medium at the highest concentrations tested (typically 200 µM of compound corresponding to 2% DMSO in the medium) which prevented us from performing the downstream experiments to identify resistant strains and suggest import routes. To propose possible transport routes for all the other compounds tested, we evaluated the results obtained from both low- and high-throughput assays (Table 1). In addition, we

275 performed high-density plate-based assays with 308 strains selected from the double-
276 deletion library to evaluate the profile of resistance in the presence of the xenobiotics
277 tested. We highlight below some interesting results and propose transporter
278 relationships for some compounds.
279
280 Tunicamycin is a nucleoside antibiotic that inhibits N-glycosylation of asparagine in
281 eukaryotes and the use of this substance is important for the study of the UPR (unfolded
282 protein response) signaling network (27). In the plate assay, we identified Fur4p as a
283 possible tunicamycin carrier, since its deletion was present in 11 of the 20 resistant
284 colonies analyzed (Table 1). Considering the CGP assay, however, the deletion strain
285 *fur4*Δ did not appear significantly abundant (Table 1). However, in the high-density
286 assay, the double mutant *pdr5::natMX fur4::kanMX* showed a resistant phenotype (F18;
287 Figure S2). The reciprocal double mutant, *fur4::natMX pdr5::kanMX* did not grow in
288 either the treatment or control plates (I03; Figure S2). It is possible to identify a plate
289 effect in this row, in which more double mutants show resistance, and this result should
290 be carefully evaluated. Fur4p acts as a uracil permease (28, 29), which indicates that its
291 contribution to the entry of the compound tunicamycin may be due to interaction with
292 the uracil moiety present in the structure of this compound. In a previous study (8), the
293 transporters Lem3p, Dnf2p, and Qdr2p were identified as responsible for the entry of
294 tunicamycin into the cell. The absence of Lem3 and Dnf2 transporters in the double-
295 mutant library tested in our work and of *fur4*Δ among the deletions tested previously (8)

296 prevents the cross-validation of the two results. Thus, the previous and current results
297 indicate the involvement of Dnf2p, Lem3p and Fur4p in the uptake of tunicamycin.
298
299 Tamoxifen is an anti-tumorigenic selective estrogen receptor modulator (30, 31). The
300 plate assay and the high-density assay revealed that deletions of the *TPO5* and *NHA1*
301 genes resulted in resistance to the compound in solid medium (Table 1; Figure S3).
302 Nha1p acts as a cation antiporter (32–34) and Tpo5p is a putrescine and spermidine
303 exporter; however, it localizes to the Golgi and post-Golgi vesicles (35). In the high-
304 density assay, however, only the double mutant *tpo5::natMX nha1::kanMX* showed a
305 resistance phenotype, and the strain *nha1::natMX tpo5::kanMX* was not resistant
306 (Figure S3). It is important to note that the deletion *nha1::kanMX* appears in other
307 resistant strains obtained in the high-density assay, which may indicate that the
308 resistance is due to a strain background effect and not a specific consequence of the
309 transporter deletion. To investigate this possibility, we performed spot tests with
310 *nha1::kan*MX and *nha1::nat*MX mutants in combination with 12 different transporters
311 and *his3* as negative control (data not shown). In all cases, we observed that
312 *nha1::kan*MX conferred resistance to tamoxifen whereas the same was not always
313 evident for *nha1::nat*MX. *nha1::nat*MX was resistant to tamoxifen in combination with
314 approximately 50% of the transporter deletions tested: *itr1::kan*MX, *tpo5::kan*MX,
315 *mal11::kan*MX, *zrc1::kan*MX, *dnf1::kan*MX, or *fcy2::kan*MX (none of which was
316 previously identified as resistant to the drug). This suggests that there could have been a
317 mutation in the original *nha1::nat*MX that leads to an increased sensitivity to tamoxifen

and is present in half of the spores produced in the library. The same pattern was not evident for azoles. Considering the CGP assay, the most abundant strains (log_2 fold change ≥ 0.5) in the tamoxifen-treated pool were the *adp1*Δ and *tna1*Δ mutants (Table 1). Adp1 is a putative ATP-dependent permease (36) and Tna1p is a high-affinity nicotinic acid permease (37). Although the *tpo5*Δ and *nha1*Δ mutants had a log_2 fold change above zero, it was not greater than 0.5. Thus, there is a clear difference in resistance between cells grown on solid and in liquid media.

Carbendazim is a benzimidazolic carbamate fungicide that acts by inhibiting the polymerization of microtubules by interaction with β-tubulin (38). Some carrier deletions were found as resistant strains in the plate assay and among the abundant strains of the CGP (Table 1). Considering those with a log_2 fold change ≥ 0.5, we have: *tna1*Δ*, nft1*Δ*, nha1*Δ*,* and *pdr5*Δ; with a log_2 fold change between 0 < 0.5: *yor1*Δ*, ady2*Δ*,* and *ybt1*Δ. Tna1p is a high-affinity transporter of nicotinic acid, a pyridinecarboxylic acid (37), and may be directly involved in the entry of carbendazim. It is worth noting the presence of the carboxylic acid group among the natural substrates for transporters identified as hits for carbendazim, as nicotinic acid for Tna1p and acetate for Ady2p. On the other hand, Nha1p may only make an indirect contribution to the drug's ingress due to its function as a cation antiporter. It is noteworthy that, we identified the ABC family members Yor1p, Ybt1p and Nft1p (multidrug resistance protein - MRP-subfamily) (23, 39), as putative importers. We also identified Pdr5p as a putative importer of carbendazim, which is interesting since this protein is typically described as an exporter.

Validation plate assays using the single-mutant *pdr5*Δ growing in an inhibitory concentration of carbendazim (data not shown) indicated that this deletion provides resistance to this compound, corroborating the involvement of Pdr5p in carbendazim uptake.

We performed validation experiments to investigate the resistance of double mutants enriched in CGP to 1,10-phenanthroline (Figure 7). Amongst the strains enriched in the CGP were *fui1*Δ, *arn1*Δ, *arn2*Δ, and *enb1*Δ. Fui1p is a high affinity uridine permease and the transporters Arn1p, Arn2p and Enb1p have similar cargo specificity (ARN family transports siderophore-iron chelates and Enb1p transports ferric enterobactin) whereas Ftr1p is a high-affinity iron permease, which is also involved in iron homeostasis. However, *ftr1*Δ strains were depleted in CGP assays. Even though Arn1p, Arn2p, Enb1p, and Ftr1p are iron transporters, only the transporters with specificity for large molecules, such as Arn1p, Arn2p, Enb1p, and Fui1p appear to contribute to 1,10-phenanthroline transport. Single transporter deletions or deletions in combination with *ftr1*Δ do not confer resistance probably due to redundancy. Only with the deletion of at least 2 of the 4 suggested transporters can we limit the compound's uptake to confer measurable resistance. Our results demonstrate the power of the double-mutant deletion library in identifying groups of transporters that contribute to the import of the test compound.

Validation of transporter-mediated import routes of Azoles

With the exception of fluconazole, azole compounds showed very consistent results with regards to their import and export routes (evident in the PCA plot, Figure 6). Azoles are antifungal agents that target the ergosterol (sterol) biosynthesis pathway by inhibiting lanosterol 14-alpha demethylase (a cytochrome p450), encoded by the *ERG11* gene in *S. cerevisiae* (21, 40, 41). When analyzing the correlation between the CGP results of six azole compounds, we found that three azole antifungals (difenoconazole, epoxiconazole, and tebuconazole) show very similar profiles of genes involved in the import and export of these compounds ($r^2 > 0.95$) (Figure 8B, C, and F). These antifungal agrochemicals are members of the 1,2,4 - triazole class and also present a halogenated benzene ring (2 in difenoconazole and epoxiconazole; 1 in tebuconazole) (Figure 8G). The azole antifungals of the imidazole class, clotrimazole and ketoconazole, are drugs for animal use and they also have a good correlation between importers and exporters ($r^2 = 0.97$) (Figure 8A and E). Fluconazole did not show any correlation with the other azoles (Figure 8D). This may be due to differences in its structure, as this compound bears an additional nitrogen-containing five-membered ring and a difluorophenyl group. These results indicate that there is a clear relationship between compound structures and the import/export routes revealed by our chemogenomic approaches. Previous studies suggested that the azoles use facilitated diffusion and that both parts of the molecule (the nitrogen-containing five-membered and the halogenated benzene rings) are essential for cell uptake (42–44). We have demonstrated that these chemical groups

show strong correlation to the substrate profile of protein transporters involved in the influx and efflux of the xenobiotics.

CGP and low-throughput assays of azole compounds showed an interesting profile of putative import and export routes (Figure 8 and Table 1), suggesting a number of carriers potentially responsible for azole uptake. The *nha1*::kan*MX* deletion mutant, for example, was a top hit for 5 of the 6 azoles tested (CGP) and *nha1*Δ deletants were identified among the resistant colonies selected in a plate assay (low-throughput assay) for clotrimazole, ketoconazole, and difenoconazole (Table 1), supporting the possible involvement of this cation antiporter in the transport of these compounds. Itr1p, which is responsible for uptake of *myo*-inositol (45), is a putative import route, as *itr1*Δ strains are resistant to the triazoles difenoconazole, epoxiconazole, and tebuconazole in both assays (Table 1). In accordance with this finding, we observed that most of the double-deletion strains resistant to triazoles in the high-density plate assay bear the deletion of the *ITR1* gene (Figure S4, Figure S5, and Figure S6). We also observed the resistance of *itr1*Δ to the imidazoles clotrimazole and ketoconazole in the high-density assay (Figure S7 and Figure S8). This is in agreement with previous work (8) in which the deletion of *ITR1* conferred resistance to the compounds clotrimazole, ketoconazole, and fluconazole in plate experiments.

Evaluating the results obtained with the compound fluconazole, an azole of the triazole class, we observe a group of transporters, the deletion of which conferred a resistance

404 phenotype in both plate and CGP approaches. The small- and large-scale screening
405 showed that the following deletions may confer resistance to this compound and thus
406 implicate the cognate transporters in the import of fluconazole: *qdr3*Δ*, tat1*Δ*, ady2*Δ*,*
407 *adp1*Δ*, yor1*Δ*, arn1*Δ*, hxt4*Δ*, bor1*Δ*,* and *hol1*Δ. We did not perform further validation
408 experiments for these transporters; however, the set of deletions that conferred
409 resistance to fluconazole are different from those observed for other azoles and may
410 contribute to the traffic of this compound.
411

412 **Itr1p is a putative azole importer**

413 We investigated the role of Itr1p on azole import by evaluating the resistance
414 phenotype of *itr1*Δ, either alone or combined with *itr2*Δ, *nha1*Δ, *pdr5*Δ mutations. Small-
415 scale assays confirmed the resistance phenotype (in plate-assays and CGP) of *itr1*Δ
416 strains to difenoconazole, epoxiconazole, ketoconazole, and tebuconazole in both solid
417 and liquid media assays (Figure 9 and data not shown). However, in the spot test, the
418 *itr1*Δ mutant did not present a strong resistance phenotype in the presence of either
419 clotrimazole or fluconazole.
420

421 Considering the important role of Pdr5p in azole efflux (20, 21), we investigated whether
422 the resistance phenotype observed for the strain was due to the absence of the
423 importer or to an activity of the exporter. We performed spot tests of BY4741 (wild
424 type) and mutant strains in the presence of sub-lethal doses of the agrochemical
425 triazoles, ketoconazole, clotrimazole, and fluconazole (Figure 9A). Our results show that

426 a cell containing all transporters (importers and exporters) is sensitive to these
427 compounds and that export pumps cannot overcome their import. The double mutant
428 *pdr5*Δ *his3*Δ was sensitive to azoles, corroborating previous findings that suggest a role
429 for this multidrug transporter in the export of azole compounds (20, 21) (Figure 9A). We
430 found that the double mutant strain *itr1*Δ *pdr5*Δ is sensitive to azoles, which indicates
431 that azoles accumulate inside the cell even in the absence of Itr1p, suggesting additional
432 import routes for azole compounds (Figure 9A). Hence, without an efficient efflux
433 through Pdr5p, the cell is susceptible to the action of azoles even when its primary
434 import route is absent.
435
436 Our approaches suggest a group of transporters that may contribute with Itr1p in azole
437 uptake. In CGP and the high-density plate-assay results, we observed that treatment
438 with the agrochemical triazoles and ketoconazole selected a set of deletions that, in
439 combination with *itr1*Δ, confer resistance phenotypes to the double mutants (Figure S4,
440 Figure S5, Figure S6, and Figure S8), namely *tpo5*Δ, *ftr1*Δ, *snq2*Δ, *smf1*Δ, *tpo1*Δ, *tna1*Δ,
441 and *adp1*Δ. We also investigated *itr2*Δ, as *ITR2* is a paralog of *ITR1,* encoding a putative
442 azole importer. However, in our plate assay (Figure 9B), the *itr2*Δ mutant did not confer
443 resistance to azoles. Nha1p was also suggested as a putative azole importer, considering
444 that *nha1*::*kanMX* was the top CGP hit for azoles and also presented as a hit in the low-
445 throughput assay (Table 1). However, validation studies with *nha1*::*natMX* showed no
446 resistance profile (Figure 9C), which may suggest that some *nha1*::*kanMX* strains might

carry additional mutations, for instance in genes specifying cytochrome P450s (46), that could be responsible for the observed phenotype.

Discussion

There is considerable controversy regarding the preferential mode of import of drugs into their target cells. The norm in the pharmaceutical industry is to design new drugs on the principle that they should be able to enter cells by passive diffusion through the plasma membrane lipid bilayer. However, this does not explain the fact that there are many efficacious drugs on the market whose physicochemical characteristics make it unlikely that they enter by this route (47). Furthermore, import by non-specific passive diffusion does not explain the differences in drug import between different tissues and, in particular, the inability of many drugs to enter the brain (2). An alternative is that, for many drugs and other xenobiotics, the primary route of ingress is likely via protein carriers located in the plasma membrane that can affect either facilitated diffusion or active transport (2, 48). In order to evaluate the primary route of import of xenobiotics and identify any transporter(s) responsible for their entry into target cells, we assembled a collection of yeast strains that lacked the genes encoding either a single or a pair of membrane transporters that can be used to rapidly evaluate whether specific transporters were involved in the import or export of individual drugs by observing the resistance phenotypes consequent on gene loss.

The library used in this work contains double-deletions of non-essential transporters, and provides at least a two-fold increase in resistant strains compared to the single-deletion library, thus enabling the identification of pairs of transporters involved in the entry of toxic compounds. Two strategies were employed for transporter identification: low-throughput (plate assay) and high-throughput assays (CGP), using a pool of the double-mutant library, combined with validation assays with isolated strains. The low-throughput approach clearly yields valuable and verifiable results; however, it is laborious and demands high sampling to obtain significant data. Alternatively, we employed high-throughput assays, where pools of double-mutant transporter-deletion strains were grown in competition and the relative contribution of each transporter to the import or export of a given test compound was inferred from the resistance (enrichment) or sensitivity (depletion) phenotypes conferred by their deletion. CGP provided quantitative clues to the relative contribution of each transmembrane protein to the transport of different compounds across the plasma membrane.

Out of 21 compounds tested in CGP in this work, 14 selected for significantly enriched strains, among which we were able to observe the same deletion strains as hits from the low- and high-throughput screens. For example, CGP, low-throughput, and high-density assays suggested putative yeast plasma membrane transporters for cytotoxic compounds and indicated that the *myo*-inositol transporter Itr1p plays a significant role in the uptake of azoles (both triazoles and imidazoles), which is in agreement with previous work that indicated the entry of azoles into the cell is via facilitated diffusion in

490 an ATP-independent process (42–44). CGP also provided consistent resistance and
491 sensitivity data for the triazole agrochemicals and the clinically important imidazoles,
492 identifying not just influx carriers, but also the efflux pumps that may export these
493 xenobiotics. We were able to identify the ABC multidrug resistance transporter Pdr5p
494 (19) as the exporter of the 6 azole compounds tested, a result consistent with previous
495 studies (20, 21). Given the importance of efflux carriers in drug resistance (49),
496 characterizing the specificity of these carriers could contribute to the development of
497 drugs refractive to transport via ABC transporters, or the development of therapies in
498 which the primary drug is used in combination with an export pump inhibitor.
499
500 Competition assays between azoles and *myo*-inositol did not confer azole resistance
501 (data not shown) and the double mutant *pdr5*Δ *itr1*Δ was also sensitive to azole
502 treatment, indicating that an alternative import route is used in the absence of Itr1p.
503 Furthermore, in spite of the evidence suggesting the import of azoles by Itr1p, the
504 deletion of *ITR2,* a paralog of *ITR1* generated by the whole-genome duplication event,
505 did not provide a resistance profile for the strain. Both transporters are responsible for
506 uptake of *myo*-inositol and have high sequence homology (45), however, our screen
507 indicates that Itr2p is unlikely to be involved in azole import. Itr1p is described as the
508 major transporter of *myo*-inositol and Itr2p plays only a minor role (45), which may
509 explain the differences in the resistance profiles observed between *itr1*Δ and *itr2*Δ
510 deletion strains.
511

In a search for transporters that may be either secondary azole transporters or have an indirect effect on these drugs' efficacy, we focused on *nha1*Δ*,* which was a recurrent hit. Nha1p is a Na^+/K^+ antiporter that acts in the active export of alkaline cations (Li^+, Na^+, K^+ and Rb^+) (32–34). It was not immediately obvious how Nha1p could be directly responsible for azole import. Hence, we performed validation experiments using the double mutants *nha1*::*natMX his3::kanMX*, *itr1::natMX nha1::kanMX,* and *nha1::natMX itr1::kanMX* (Figure 9C). Whilst the *nha1::kanMX* deletant was resistant to azoles in both low- and high-throughput assays (we were only able to track the *kan*MX barcodes), we did not observe any resistance profile for *nha1*::*natMX his3::kanMX*, a strain bearing the Itr1 transporter. Hence the presence of *nha1*Δ as a top hit may be due to additional mutations in the strain carrying *nha1::kanMX*.

Our library consists of approximately 14,000 strains constructed by crossing 122 transporter-gene deletions (*kan*MX marker with barcodes) with 120 transporter-gene deletions (*nat*MX marker without barcodes). Considering all the combinations, we have double deletions of importers and exporters that can improve the identification of transport routes*.* We believe that this strategy for identifying which transporters are involved in the transport of specific compound could be improved by performing pairwise crosses of all non-essential transporter-gene deletions (including genes not represented in our library) barcoded in both alleles to better represent all non-essential import routes and facilitate the identification of transporter pairs working in xenobiotic import. With the development of new strategies for mapping compound import and

export routes, we aim to contribute to our understanding of resistance mechanisms, which is critical for the design of drugs with continued efficacy. Furthermore, the knowledge of transporter substrate specificity may allow the design of pro-drugs with enhanced targeting to the cell type of interest. Hence, we are convinced that our double-deletion library is an invaluable tool for the design of more specific and efficient therapies.

Materials and Methods

Media

The following media were used for the construction of the double-mutant collection by SGA (50–52): YPD (2% bacto peptone, 1% yeast extract, 2% glucose, 2% agar) with G418 (200 mg/L) or clonNAT (100 mg/L); enriched sporulation medium (20 g/L agar, 10 g/L potassium acetate, 1 g/L yeast extract, 0.5 g/L glucose, 12.5 mg/L histidine, 12.5 mg/L lysine, 12.5 mg/L uracil, 62.5 mg/L leucine); selective YNB medium (6.7 g/L yeast nitrogen base with ammonium sulfate and w/o amino acids, 50 mg/L canavanine, 50 mg/L thialysine, 150 mg/L leucine, 40 mg/L uracil, 40 mg/L methionine, 2% glucose); and YNB/MSG medium (1.7 g/L yeast nitrogen base w/o ammonium sulfate and w/o amino acids, 1 g/L monosodium glutamic acid, 100 mg/L clonNAT, 200 mg/L G418, 50 mg/L canavanine, 50 mg/L thialysine, 150 mg/L leucine, 40 mg/L uracil, 40 mg/L methionine, 2% glucose).

Drug sensitivity assays for determination of the inhibitory concentrations of xenobiotics and for selection of resistant strains were performed in YNB+Sc medium (6.7 g/L yeast nitrogen base with ammonium sulfate and without amino acids, complete amino acid supplement, 2% glucose), with or without 2% bacto agar.

Commercial xenobiotics

We selected commercial xenobiotics, including agrochemicals and drugs for both human and animal use, and prepared 10 mM stock solutions (20 mM for artesunate; 40 mM for dl-4-hydroxy-3-methoxymandelic acid and tamoxifen) in 100% DMSO of the compounds purchased from Sigma-Aldrich (Merck Group) (Table S1). We selected 5-fluorocytosine (Catalog number F7129 - Sigma Aldrich, Merck Group) as a positive control for the assays as the deletion of *FCY2* (YER056C; encoding the purine-cytosine permease) is well characterized and provides a resistant phenotype to this compound (8, 53).

Strains

A double-mutant *S. cerevisiae* library was constructed by crossing single mutant strains in the BY741 (*MAT**a**; his3*Δ*1; leu2*Δ*0; met15*Δ*0; ura3*Δ*0*) background (54) with single mutant strains in the Y7092 (*MATα; can1*Δ*::STE2pr-Sp_his5; lyp1*Δ*; his3*Δ*1; leu2*Δ*0; ura3*Δ*0; met15*Δ*0*) background (51, 52). In BY4741 genetic background, one of the following plasma membrane transporter encoding genes was replaced with the antibiotic resistance marker *kan*MX, flanked by unique sequences (genetic barcodes) identifying deletions in each of the following open reading-frames: YAL067C, YBL042C,

578 YBR008C, YBR021W, YBR043C, YBR068C, YBR069C, YBR180W, YBR294W, YBR295W,
579 YBR296C, YBR298C, YCL025C, YCR010C, YCR011C, YCR028C, YCR098C, YDL199C,
580 YDR011W, YDR046C, YDR345C, YDR384C, YDR387C, YDR406W, YDR497C, YDR508C,
581 YDR536W, YEL063C, YEL065W, YER056C, YER145C, YER166W, YFL011W, YFL040W,
582 YFL050C, YFL055W, YGL077C, YGL114W, YGL255W, YGR055W, YGR121C, YGR138C,
583 YGR217W, YGR224W, YGR260W, YGR281W, YGR289C, YHL016C, YHL040C, YHL047C,
584 YHR092C, YHR094C, YHR096C, YIL013C, YIL088C, YIL120W, YIL121W, YJL093C, YJL129C,
585 YJL212C, YJL214W, YJR040W, YJR054W, YJR152W, YKL174C, YKL217W, YKR039W,
586 YKR050W, YKR103W, YKR106W, YLL028W, YLL043W, YLL048C, YLL052C, YLL061W,
587 YLR081W, YLR092W, YLR130C, YLR138W, YLR237W, YML047C, YML116W, YML123C,
588 YMR011W, YMR177W, YMR243C, YMR279C, YMR319C, YNL065W, YNL142W, YNL268W,
589 YNL270C, YNL275W, YNL291C, YNL318C, YNR002C, YNR055C, YNR056C, YNR072W,
590 YOL020W, YOL103W, YOL122C, YOL158C, YOR011W, YOR071C, YOR153W, YOR192C,
591 YOR202W, YOR273C, YOR306C, YOR328W, YOR348C, YPL036W, YPL058C, YPL092W,
592 YPL265W, YPL274W, YPR124W, YPR138C, YPR156C, YPR192W, YPR198W, YPR201W
593 (55). In the Y7092 background, the same plasma membrane transporter-encoding genes
594 (except YEL063C, YHR096C and YOR202W) were replaced with the *nat*MX marker (50).
595 In the library construction, strains containing deletions of genes non-related to transport
596 (YAL060W, YDR073W, and YIR002C) were added as negative controls.
597

598 **Construction of the transporter double-mutant library by Synthetic Genetic Array**

599 The construction of the transporter double-mutant collection library was
600 performed essentially as described by Tong and coworkers (50–52). Briefly, 122
601 transporter-encoding genes deletion strains (plus the control strain with YOR202W
602 deletion), in the BY741 background (54) were grown in 384-colony arrays (pinned using
603 the Singer Rotor HAD, Singer Instruments, UK) on YPD with G418 (200 mg/L) for 1 day at
604 30^{o}C. In parallel, 120 strains in the Y7092 background (51, 52) were grown in 384-colony
605 arrays on YPD with clonNAT (100 mg/L) for 1 day at 30^{o}C. Strains of opposite mating
606 type were then pinned onto fresh YPD plates and allowed to mate at room temperature
607 for 24 hours. They were then pinned onto YPD+G418+clonNAT and incubated at 30^{o}C for
608 2 days to select for diploid cells. The diploids were then pinned onto enriched
609 sporulation medium and incubated at room temperature for 5-10 days. The *MAT**a***
610 meiotic progeny were selected by pinning the sporulated strains onto selective SD
611 medium and incubated at 30^{o}C for 2 days. Transporter double-mutant *MAT**a*** strains
612 were then selected by pinning onto SD/MSG medium and incubating at 30^{o}C for 2 days.
613 This last step was repeated to ensure that all strains were indeed double mutants.
614 Double mutants were replicated into 384-well plates with YPD + 15% v/v glycerol and
615 stored at - 80^{o}C. Double mutants were also pooled in the ratio of 1:1:1:1:…:1 and stored
616 in YPD + 15% v/v glycerol in 5 mL aliquots for competition experiments (library pools).
617 The transporter-deletion library constructed during the current study will be deposited
618 with EUROSCARF.

619

Determination of inhibitory concentrations of commercial xenobiotics

S. cerevisiae BY4741 was inoculated into 5 mL of fresh YNB+Sc and grown overnight at 30°C with agitation. Then the culture was diluted to OD_{595} 0.1 in 70 µL of YNB+Sc containing different dilutions of each xenobiotic. The xenobiotics were tested in the following concentrations: 200 µM, 100 µM, 40 µM, 20 µM, 8 µM, 4 µM, 1.6 µM, 0.8 µM, 0.32 µM and 0.16 µM. Controls containing 2% and 1% DMSO (v/v) were also tested. Cultures were prepared in quadruplicate in 384-well flat bottom plates and incubated at 30°C, with linear shaking (700 rpm) in the CLARIOstar® (BMG Labtech) plate reader, for 30 hours with OD_{595} measurements every 10 minutes. Curves derived from the growth data were smoothed based on the moving average of the 15 closest measurements, and the growth score was calculated by multiplying the yield (OD_{max} – OD_{min}) by the maximum slope of the curve and dividing by the time taken to reach the maximum slope, using the data analysis software MARS (BMG Labtech). Non-linear regression for IC_{90} definition was performed using GraphPad Prism version 8.0.0 for Windows, GraphPad Software, San Diego, California USA.

Spot assays were performed in Petri dishes (90 x 15 mm) containing YNB+Sc with inhibitory concentrations of a xenobiotic, as defined by growth assays in liquid cultures, with equivalent volumes of DMSO in negative control plates. Serial dilutions (1:5 dilution) of BY4741, single- and double-mutant library pool and selected single-mutant strains were spotted onto control or xenobiotic containing plates for selective inhibition verification and, for definition of inhibitory concentrations, onto solid media using 48-

642 pin replicators (Sigma-Aldrich, Merck Group). Plates were incubated at 30°C for 2-4 days,
643 and images were registered with ChemiDoc™ MP (Bio-Rad).
644
645 **Selection of resistant strains**
646 Assays were performed on Petri plates (90 x 15 mm) containing YNB+Sc agar with
647 inhibitory concentration of xenobiotics. Onto these plates, approximately 10^3, 10^4, 10^5,
648 and 10^6 CFU of BY4741 or the double-mutant library pool were plated. Plates containing
649 YNB+Sc with DMSO were used as plating controls. After 2 days of incubation at 30ºC,
650 growth was registered with ChemiDoc™ MP (Bio-Rad) and resistant colonies from library
651 pool plates were picked and transferred to fresh non-selective plates.
652
653 **Identification of resistant strains**
654 Genomic DNA was prepared as described in Lõoke *et al.,* 2011 (56). Cells from resistant
655 colonies were lysed by resuspension into 100 µL of 200 mM LiAc with 1% SDS, followed
656 by incubation at 70°C for 15 minutes. DNA was precipitated by the addition of 300 µL
657 100% ethanol, followed by briefly vortexing and centrifugation for 3 minutes at 15,000
658 g. Pellets were washed with 200 µL 70% v/v ethanol, centrifuged for 3 minutes at 15,000
659 g and air-dried. gDNA pellets were dissolved in 100 µL of ultrapure water, followed by
660 centrifugation for 15 seconds at 15,000 g. PCR reactions using Taq DNA Polymerase
661 P1011 (Sinapse Inc) were prepared following the manufacturer's instructions. Barcode
662 amplification was performed using primers pairs U1 forward 5'-
663 GATGTCCACGAGGTCTCT-3' with *kan*MX reverse 5'-CATCATTGGCAACGCTAC-3'

(upstream barcode) or *kan*MX forward 5'-CTCCTTCATTACAGAAACGG-3' with D1 reverse 5'-CGGTGTCGGTCTCGTAG-3' (downstream barcode). PCR products were purified using the E.Z.N.A.® Gel Extraction Kit (OMEGA Bio-tek) and sequenced by Sanger Sequencing. For upstream barcode sequencing, primer pTEF seq reverse 5'- CGACAGTCACATCATGCC-3' was used and for downstream barcode sequencing, primer *kan*MX forward was used. Sequencing was performed at Myleus Biotechnology using capillary electrophoresis (ABI3730) using POP7 polymer and BigDye v3.1. Sequence analyses and barcode identification was performed based on *Saccharomyces* Genome Deletion Project barcode list (18).

Chemical genomic profiling

Determination of the inhibitory concentration of xenobiotics for transporter deletion strains was accomplished by growth curve assays of library pools. These were performed in liquid media in 48-well flat bottom plates with incubation at 30^{o}C, with 500 rpm double orbital shaking in the CLARIOstar® (BMG Labtech) plate reader, for 48 hours with OD_{595} measurements every 10 minutes. Concentrations selected for chemical genomic profiling were those that inhibited growth of transporter-deletion pools by approximately 80% whilst allowing the culture to reach the stationary phase in 24 hours.

The transporter double-deletion library pool was grown in YNB+Sc for 12 hours at 30°C with agitation. Pools were then diluted to OD_{600} 0.1 in 500 µL of YNB+Sc containing the xenobiotic compounds in 48-well flat bottom plates (samples were prepared in

686 quadruplicate). After 24 hours growth at 30°C with agitation (ca. 5 generations), OD_{595}
687 was measured, and cultures were diluted 20x in 500 µL of fresh media containing the
688 xenobiotic and allowed to grow for 12 hours (ca. 10 generations) under the same
689 conditions. The dilution procedure was repeated, and cultures were allowed to grow
690 until stationary phase (ca. 15 generations). Cell pellets were collected, and genomic DNA
691 was extracted using the Wizard® Genomic DNA Purification Kit. Upstream barcodes
692 were PCR amplified with U1 and U2 primers containing Illumina pre-adaptors for
693 multiplex barcode sequencing with Illumina HiSeq2500 platform by the University of São
694 Paulo Functional Genomics Center.
695
696 The quality of the generated reads was analyzed with the FastQC (version 0.11.7) (57)
697 and MultiQC (version 1.6) (58) software before and after removal of primers and
698 adapters performed with the Cutadapt tool (version 1.26) (59). DADA2 (version 1.9.1)
699 (60) was employed to infer amplicon sequencing variants (ASVs) by trimming and
700 discarding low-quality reads, correcting sequencing errors (denoising) and merging read
701 pairs. Since it is known that several barcodes have sequences different from those that
702 were originally described (61), ASVs that did not match any previously described
703 barcode were assigned to the most similar barcode sequencing if the Levenshtein
704 distance was equal to or less than 2. If two or more ASVs matched the same barcode,
705 the read counts of those ASVs were combined. With the DESeq2 package (version
706 1.20.0) (62), the normalization of counts and the assessment of the differential
707 abundance of barcodes between samples treated against untreated controls were

performed. For principal components analysis (PCA), the barcode count matrix was transformed using the rlog function to standardize the abundance variance between the different barcodes. Differentially abundant strains were identified using a maximum likelihood ratio test and normalization between samples was done by the library size factor method (63). Differentially abundant barcodes in treated versus control comparisons were considered significant for the p-value adjusted for multiple tests (padj) by the Benjamini-Hochberg method (≤ 0.1) and p-value less than 0.001. For the analysis, we used thresholds of $\log_2$ fold change at ≥ 0.5 (for resistant strains) and ≤ -0.5 (for sensitive strains). Correlation from 116 genes presented in all azoles data from CGP was performed using GraphPad Prism version 8.0.0 for Windows, GraphPad Software, San Diego, California USA. CGP datasets with differential abundance of barcodes are presented in Data set S1.

High-density plate assays for transporter validation

Based on chemical-genomic results, 308 double-transporter-deletion mutants were selected for validation (padj ≤ 0,1; p-value ≤ 0,001; $\log_2$ fold change ≥ 0,5). These were inoculated in 50 µL of YNB + Sc liquid medium in a 384-well plate and grown at 30°C until saturation (~ 36 hours). Using the Rotor HDA (Singer Instruments, UK), cultures were stamped in quadruplicate (1536 spots) on plates containing solid YNB+Sc medium at inhibitory concentrations (1x and 2x) of the test compounds. Cultures were incubated for 2 days at 30°C and on subsequent days at room temperature (~25°C). Plate photos were registered with ChemiDoc™ MP (Bio-Rad).

Quantification of the growth of strains was performed by analyzing the images in .jpg format using a python script. The OpenCV package contour detection module for python was used to delimit the plate and some colonies in the image. Based on this, the identification of the 1536 spots and delimitation of the columns and lines of the plate was performed. Voids (16 spots without culture inoculation; 4 corners of the plate) and wild type 288 spots (BY4741; plate edge) were identified. For each spot, a quadrangular cut-out of a fixed area was delimited. To estimate the growth in the spot, the pixel values in this cut-out were averaged, considering the black and white scale (values from 0 to 255). For each strain, the median of the 4 values was calculated according to the plate map. The z-score was calculated using median values, according to the median of a sample minus the mean of all median values, divided by the standard deviation of all median values. Strains that varied by more than 3 standard deviations (3*SD) from the mean were considered resistant.

Small-scale validation assays

Gene deletion of strains selected for validation were confirmed by PCR with "A_confirmation_primer" (18) and *kan*MX reverse 5'-CATCATTGGCAACGCTAC-3' (for *kan*MX gene deletion) or *nat*MX reverse 5'-AAGACGGTGTCGGTGGTG-3' (for *nat*MX gene deletion). Overnight cultures in YNB+Sc were serial diluted in a 96-well plate and stamped using a Replica plater with 48 pins (Sigma-Aldrich, Merck Group) in Petri dishes with solid media YNB+Sc containing inhibitory concentrations of xenobiotics. Cultures

were incubated for 2 days at 30°C and on subsequent days incubated at room temperature (~25°C). Plate photos were registered with ChemiDoc™ MP (Bio-Rad). Growth curves and non-linear regression of selected deletants were performed as described for IC_{90} determination.

Data availability

High-throughput sequencing data of the CGP screens have been deposited in the NCBI Short Read Archive (SRA) under BioProject PRJNA718573 (BioSamples SAMN18541664 to SAMN18541685).

Acknowledgements

This work was supported by Fundação de Amparo à Pesquisa do Estado de São Paulo (FAPESP – EB Grant 2015/03553-6), by The Bill and Melinda Gates Foundation Grand Challenges Explorations (Grant OP1087646), and by UK Biotechnology and Biological Sciences Research Council (Grant BB/F008228/1 to SGO). LDA was supported by FAPESP (2017/01986-8) and by the Coordenação de Aperfeiçoamento de Pessoal de Nível Superior - Brasil (CAPES - Finance Code 001) fellowships. ASFS, GSP and HMRCF were supported by a FAPESP fellowship (2019/14146-3, 2018/05328-8 and 2019/17876-2, respectively). AAV and APC were supported by a FAPESP fellowship (2017/13015-7 and 2018/04240-0, respectively). AHK was supported by a FAPESP fellowship (2018/16672-1). We thank the funding agencies, FAPESP, The Bill and Melinda Gates Foundation, UK

773 Biotechnology and Biological Sciences Research Council, and CAPES, for financial
774 support. The funding agencies had no role in the study design, data collection and
775 interpretation, and in the decision to submit the paper for publication.

776

777 We thank the Charles Boone lab for the *nat*MX deletion strains used in the library
778 construction, and Douglas Bruce Kell for helpful discussions.

779

780 EB constructed the double-mutant library. LDA, ASFS, and DCM defined xenobiotic
781 inhibitory concentration. LDA, ASFS, DCM, GSP, and MF performed the low-throughput
782 plate assay and strain identification. LDA, HMRCF, AAV, APC, and MFC performed the
783 chemical genomic profiling and subsequent analysis. LDA, ASFS, AHK, SFS, and CFZ
784 performed the high-density plate assay and subsequent analysis. LDA performed the
785 validation assays. LDA and EB analyzed all data and proposed transport routes. EB, SGO,
786 and LDA conceived the project, supervised research, and wrote the manuscript. All
787 authors revised and approved the manuscript.

788

789 **List of abbreviations**

790 ABC: ATP-Binding Cassette

791 CFUs: Colony-Forming Units

792 CGP: Chemical Genomic Profiling

793 HIP: Haploinsufficiency Profiling

794 HOP: Homozygous Deletion Profiling

795 KO: Knockout

796 MFS: Major Facilitator Superfamily

797 padj: p-value adjusted for multiple tests

798 PCA: Principal Components Analysis

799 SD: Standard Deviation

800 SGA: Synthetic Genetic Arrays

801 SLCs: Solute Carrier

802 UPR: Unfolded Protein Response

803

804

805

References

1. Kell DB, Dobson PD, Oliver SG. 2011. Pharmaceutical drug transport: The issues and the implications that it is essentially carrier-mediated only. Drug Discov Today 16:704–714.
2. Kell DB, Dobson PD, Bilsland E, Oliver SG. 2013. The promiscuous binding of pharmaceutical drugs and their transporter-mediated uptake into cells: What we (need to) know and how we can do so. Drug Discov Today 18:218–239.
3. König J, Müller F, Fromm MF. 2013. Transporters and drug-drug interactions: Important determinants of drug disposition and effects. Pharmacol Rev 65:944–966.
4. Kell DB, Oliver SG. 2014. How drugs get into cells: tested and testable predictions to help discriminate between transporter-mediated uptake and lipoidal bilayer diffusion. Front Pharmacol 5:1–32.
5. Nigam SK. 2014. What do drug transporters really do? Nat Rev Drug Discov 14:29–44.
6. Mao Q, Lai Y, Wang J. 2018. Drug transporters in xenobiotic disposition and pharmacokinetic prediction. Drug Metab Dispos 46:561–566.
7. Superti-Furga G, Lackner D, Wiedmer T, Ingles-Prieto A, Barbosa B, Girardi E, Goldmann U, Gürtl B, Klavins K, Klimek C, Lindinger S, Liñeiro-Retes E, Müller AC, Onstein S, Redinger G, Reil D, Sedlyarov V, Wolf G, Crawford M, Everley R, Hepworth D, Liu S, Noell S, Piotrowski M, Stanton R, Zhang H, Corallino S, Faedo A, Insidioso M, Maresca G, Redaelli L, Sassone F, Scarabottolo L, Stucchi M,

828 Tarroni P, Tremolada S, Batoulis H, Becker A, Bender E, Chang YN, Ehrmann A,
829 Müller-Fahrnow A, Pütter V, Zindel D, Hamilton B, Lenter M, Santacruz D, Viollet
830 C, Whitehurst C, Johnsson K, Leippe P, Baumgarten B, Chang L, Ibig Y, Pfeifer M,
831 Reinhardt J, Schönbett J, Selzer P, Seuwen K, Bettembourg C, Biton B, Czech J, de
832 Foucauld H, Didier M, Licher T, Mikol V, Pommereau A, Puech F, Yaligara V,
833 Edwards A, Bongers BJ, Heitman LH, IJzerman AP, Sijben HJ, van Westen GJP,
834 Grixti J, Kell DB, Mughal F, Swainston N, Wright-Muelas M, Bohstedt T, Burgess-
835 Brown N, Carpenter L, Dürr K, Hansen J, Scacioc A, Banci G, Colas C, Digles D,
836 Ecker G, Füzi B, Gamsjäger V, Grandits M, Martini R, Troger F, Altermatt P,
837 Doucerain C, Dürrenberger F, Manolova V, Steck AL, Sundström H, Wilhelm M,
838 Steppan CM. 2020. The RESOLUTE consortium: unlocking SLC transporters for
839 drug discovery. Nat Rev Drug Discov 19:429–430.
840 8. Lanthaler K, Bilsland E, Dobson PD, Moss HJ, Pir P, Kell DB, Oliver SG. 2011.
841 Genome-wide assessment of the carriers involved in the cellular uptake of drugs:
842 a model system in yeast. BMC Biol 9:1–14.
843 9. Girardi E, César-Razquin A, Lindinger S, Papakostas K, Konecka J, Hemmerich J,
844 Kickinger S, Kartnig F, Gürtl B, Klavins K, Sedlyarov V, Ingles-Prieto A, Fiume G,
845 Koren A, Lardeau CH, Kumaran Kandasamy R, Kubicek S, Ecker GF, Superti-Furga
846 G. 2020. A widespread role for SLC transmembrane transporters in resistance to
847 cytotoxic drugs. Nat Chem Biol 16:469–478.
848 10. Wang G, Møller-Hansen I, Babaei M, D'Ambrosio V, Christensen HB, Darbani B,
849 Jensen MK, Borodina I. 2021. Transportome-wide engineering of Saccharomyces

cerevisiae. Metab Eng 64:52–63.

11. Hillenmeyer ME, Fung E, Wildenhain J, Pierce SE, Hoon S, Lee W, Proctor M, St.Onge RP, Tyers M, Koller D, Altman RB, Davis RW, Nislow C, Giaever G. 2008. The chemical genomic portrait of yeast: uncovering a phenotype for all genes. Science 320:362–365.

12. Hoepfner D, Helliwell SB, Sadlish H, Schuierer S, Filipuzzi I, Brachat S, Bhullar B, Plikat U, Abraham Y, Altorfer M, Aust T, Baeriswyl L, Cerino R, Chang L, Estoppey D, Eichenberger J, Frederiksen M, Hartmann N, Hohendahl A, Knapp B, Krastel P, Melin N, Nigsch F, Oakeley EJ, Petitjean V, Petersen F, Riedl R, Schmitt EK, Staedtler F, Studer C, Tallarico JA, Wetzel S, Fishman MC, Porter JA, Movva NR. 2014. High-resolution chemical dissection of a model eukaryote reveals targets, pathways and gene functions. Microbiol Res 169:107–120.

13. Lee AY, St.Onge RP, Proctor MJ, Wallace IM, Nile AH, Spagnuolo PA, Jitkova Y, Gronda M, Wu Y, Kim MK, Cheung-Ong K, Torres NP, Spear ED, Han MKL, Schlecht U, Suresh S, Duby G, Heisler LE, Surendra A, Fung E, Urbanus ML, Gebbia M, Lissina E, Miranda M, Chiang JH, Aparicio AM, Zeghouf M, Davis RW, Cherfils J, Boutry M, Kaiser CA, Cummins CL, Trimble WS, Brown GW, Schimmer AD, Bankaitis VA, Nislow C, Bader GD, Giaever G. 2014. Mapping the cellular response to small molecules using chemogenomic fitness signatures. Science 344:208–211.

14. Chartier M, Morency LP, Zylber MI, Najmanovich RJ. 2017. Large-scale detection of drug off-targets: Hypotheses for drug repurposing and understanding side-effects. BMC Pharmacol Toxicol 18:1–16.

872 15. Jindal S, Yang L, Day PJ, Kell DB. 2019. Involvement of multiple influx and efflux
873 transporters in the accumulation of cationic fluorescent dyes by Escherichia coli.
874 BMC Microbiol 19:1–16.
875 16. Cherry JM, Hong EL, Amundsen C, Balakrishnan R, Binkley G, Chan ET, Christie KR,
876 Costanzo MC, Dwight SS, Engel SR, Fisk DG, Hirschman JE, Hitz BC, Karra K, Krieger
877 CJ, Miyasato SR, Nash RS, Park J, Skrzypek MS, Simison M, Weng S, Wong ED.
878 2012. Saccharomyces Genome Database: the genomics resource of budding
879 yeast. Nucleic Acids Res 40:D700–D705.
880 17. Lipinski CA, Lombardo F, Dominy BW, Feeney PJ. 1997. Experimental and
881 computational approaches to estimate solubility and permeability in drug
882 discovery and development settings. Adv Drug Deliv Rev 23:3–25.
883 18. Saccharomyces Genome Deletion Project.
884 19. Kolaczkowski M, Kolaczkowska A, Luczynski J, Witek S, Goffeau A. 1998. In vivo
885 characterization of the drug resistance profile of the major ABC transporters and
886 other components of the yeast pleiotropic drug resistance network. Microb Drug
887 Resist 4:143–158.
888 20. Rogers B, Decottignies A, Kolaczkowski M, Carvajal E, Balzi E, Goffeau A. 2001. The
889 pleitropic drug ABC transporters from Saccharomyces cerevisiae. J Mol Microbiol
890 Biotechnol 3:207–214.
891 21. Demuyser L, Van Dijck P. 2019. Can Saccharomyces cerevisiae keep up as a model
892 system in fungal azole susceptibility research? Drug Resist Updat 42:22–34.
893 22. Wilcox LJ, Balderes DA, Wharton B, Tinkelenberg AH, Rao G, Sturley SL. 2002.

894 Transcriptional profiling identifies two members of the ATP-binding cassette
895 transporter superfamily required for sterol uptake in yeast. J Biol Chem
896 277:32466–32472.
897 23. Mason DL, Mallampalli MP, Huyer G, Michaelis S. 2003. A region within a lumenal
898 loop of Saccharomyces cerevisiae Ycf1p directs proteolytic processing and
899 substrate specificity. Eukaryot Cell 2:588–598.
900 24. Cannon RD, Lamping E, Holmes AR, Niimi K, Baret P V, Keniya M V, Tanabe K,
901 Niimi M, Goffeau A, Monk BC. 2009. Efflux-mediated antifungal drug resistance.
902 Clin Microbiol Rev 22:291–321.
903 25. Sá-Correia I, dos Santos SC, Teixeira MC, Cabrito TR, Mira NP. 2009. Drug:H+
904 antiporters in chemical stress response in yeast. Trends Microbiol 17:22–31.
905 26. Alarco A-M, Balan I, Talibi D, Mainville N, Raymond M. 1997. AP1-mediated
906 multidrug resistance in Saccharomyces cerevisiae requires FLR1 encoding a
907 transporter of the major facilitator superfamily. J Biol Chem 272:19304–19313.
908 27. Heifetz A, Keenan RW, Elbein AD. 1979. Mechanism of action of tunicamycin on
909 the UDP-GlcNAc:dolichyl-phosphate GlcNAc-1-phosphate transferase.
910 Biochemistry 18:2186–2192.
911 28. Jund R, Weber E, Chevallier M-R. 1988. Primary structure of the uracil transport
912 protein of Saccharomyces cerevisiae. Eur J Biochem 171:417–424.
913 29. Chevallier MR. 1982. Cloning and transcriptional control of a eucaryotic permease
914 gene. Mol Cell Biol 2:977–984.
915 30. Shagufta IA. 2018. Tamoxifen a pioneering drug: An update on the therapeutic

potential of tamoxifen derivatives. Eur J Med Chem 143:515–531.

31. Cronin-Fenton DP, Damkier P. 2018. Tamoxifen and CYP2D6: A controversy in pharmacogenetics, p. 65–91. *In* Brøsen, K, Damkier, P (eds.), Advances in Pharmacology. Elsevier, San Diego.

32. Prior C, Potier S, Souciet JL, Sychrova H. 1996. Characterization of the NHA1 gene encoding a Na+/H+-antiporter of the yeast Saccharomyces cerevisiae. FEBS Lett 387:89–93.

33. Bañuelos MA, Sychrová H, Bleykasten-Grosshans C, Souciet J, Potier S. 1998. The Nhal antiporter of Saccharomyces cerevisiae mediates sodium and potassium efflux. Microbiology 144:2749–2758.

34. Kinclová O, Ramos J, Potier S, Sychrová H. 2001. Functional study of the Saccharomyces cerevisiae Nha1p C-terminus. Mol Microbiol 40:656–668.

35. Tachihara K, Uemura T, Kashiwagi K, Igarashi K. 2005. Excretion of putrescine and spermidine by the protein encoded by YKL174c (TPO5) in Saccharomyces cerevisiae. J Biol Chem 280:12637–12642.

36. Decottignies A, Goffeau A. 1997. Complete inventory of the yeast ABC proteins. Nat Genet 15:137–145.

37. Llorente B, Dujon B. 2000. Transcriptional regulation of the Saccharomyces cerevisiae DAL5 gene family and identification of the high affinity nicotinic acid permease TNA1 (YGR260w). FEBS Lett 475:237–241.

38. Davidse LC. 1986. Benzimidazole fungicides: mechanism of action and biological impact. Annu Rev Phytopathol 24:43–65.

938 39. Jungwirth H, Kuchler K. 2006. Yeast ABC transporters – A tale of sex, stress, drugs
939 and aging. FEBS Lett 580:1131–1138.
940 40. Kelly SL, Arnoldi A, Kelly DE. 1993. Molecular genetic analysis of azole antifungal
941 mode of action. Biochem Soc Trans 21:1034–1038.
942 41. Zavrel M, White TC. 2015. Medically important fungi respond to azole drugs: an
943 update. Future Microbiol 10:1355–1373.
944 42. Mansfield BE, Oltean HN, Oliver BG, Hoot SJ, Leyde SE, Hedstrom L, White TC.
945 2010. Azole drugs are imported by facilitated diffusion in Candida albicans and
946 other pathogenic fungi. PLoS Pathog 6:1–11.
947 43. Esquivel BD, Smith AR, Zavrel M, White TC. 2015. Azole drug import into the
948 pathogenic fungus Aspergillus fumigatus. Antimicrob Agents Chemother 59:3390–
949 3398.
950 44. Esquivel BD, White TC. 2017. Accumulation of azole drugs in the fungal plant
951 pathogen Magnaporthe oryzae is the result of facilitated diffusion influx. Front
952 Microbiol 8:1–12.
953 45. Nikawa JI, Tsukagoshi Y, Yamashita S. 1991. Isolation and characterization of two
954 distinct myo-inositol transporter genes of Saccharomyces cerevisiae. J Biol Chem
955 266:11184–11191.
956 46. Parker JE, Merkamm M, Manning NJ, Pompon D, Kelly SL, Kelly DE. 2008.
957 Differential azole antifungal efficacies contrasted using a Saccharomyces
958 cerevisiae strain humanized for sterol 14 alpha-demethylase at the homologous
959 locus 52:3597–3603.

960 47. Zhang M-Q, Wilkinson B. 2007. Drug discovery beyond the 'rule-of-five.' Curr Opin
961 Biotechnol 18:478–488.
962 48. Pizzagalli MD, Bensimon A, Superti-Furga G. 2020. A guide to plasma membrane
963 solute carrier proteins. FEBS J 1–52.
964 49. Cowen LE, Sanglard D, Howard SJ, Rogers PD, Perlin DS. 2015. Mechanisms of
965 antifungal drug resistance. Cold Spring Harb Perspect Med 5:1–22.
966 50. Tong AHY, Evangelista M, Parsons AB, Xu H, Bader GD, Pagé N, Robinson M,
967 Raghibizadeh S, Hogue CWV, Bussey H, Andrews B, Tyers M, Boone C. 2001.
968 Systematic genetic analysis with ordered arrays of yeast deletion mutants.
969 Science 294:2364–2368.
970 51. Tong AHY, Boone C. 2006. Synthetic genetic array analysis in Saccharomyces
971 cerevisiae, p. 171–191. *In* Xiao, W (ed.), Yeast Protocol. Methods in Molecular
972 Biology. Humana Press, Totowa.
973 52. Tong AHY, Boone C. 2007. High-throughput strain construction and systematic
974 synthetic lethal screening in Saccharomyces cerevisiae, p. 369–707. *In* Stansfield,
975 I, Stark, MJR (eds.), Yeast Gene Analysis Methods in Microbiology. Elsevier, New
976 York.
977 53. Guetsova ML, Lecoq K, Daignan-Fornier B. 1997. The isolation and
978 characterization of Saccharomyces cerevisiae mutants that constitutively express
979 purine biosynthetic genes. Genetics 147:383–397.
980 54. Brachmann CB, Davies A, Cost GJ, Caputo E, Li J, Hieter P, Boeke JD. 1998.
981 Designer deletion strains derived from Saccharomyces cerevisiae S288C: A useful

982 set of strains and plasmids for PCR-mediated gene disruption and other
983 applications. Yeast 14:115–132.
984 55. Giaever G, Shoemaker DD, Jones TW, Liang H, Winzeler EA, Astromoff A, Davis
985 RW. 1999. Genomic profiling of drug sensitivities via induced haploinsufficiency.
986 Nat Genet 21:278–283.
987 56. Lõoke M, Kristjuhan K, Kristjuhan A. 2011. Extraction of genomic DNA from yeasts
988 for PCR-based applications. Biotechniques 50:325–328.
989 57. Andrews S. FastQC - A quality control tool for high throughput sequence data.
990 Babraham Bioinforma.
991 58. Ewels P, Magnusson M, Lundin S, Käller M. 2016. MultiQC: Summarize analysis
992 results for multiple tools and samples in a single report. Bioinformatics 32:3047–
993 3048.
994 59. Martin M. 2011. Cutadapt removes adapter sequences from high-throughput
995 sequencing reads. EMBnet.journal 17:10–12.
996 60. Callahan BJ, McMurdie PJ, Rosen MJ, Han AW, Johnson AJA, Holmes SP. 2016.
997 DADA2: High-resolution sample inference from Illumina amplicon data. Nat
998 Methods 13:581–583.
999 61. Eason RG, Pourmand N, Tongprasit W, Herman ZS, Anthony K, Jejelowo O, Davis
1000 RW, Stolc V. 2004. Characterization of synthetic DNA bar codes in Saccharomyces
1001 cerevisiae gene-deletion strains. Proc Natl Acad Sci U S A 101:11046–11051.
1002 62. Love MI, Huber W, Anders S. 2014. Moderated estimation of fold change and
1003 dispersion for RNA-seq data with DESeq2. Genome Biol 15:1–21.

1004 63. Anders S, Huber W. 2010. Differential expression analysis for sequence count
1005 data. Genome Biol 272:1–12.

1006

1007

Figure Legends

Figure 1. **Schematic view of the experimental strategy designed to identify plasma membrane import routes.** The strategy is applied for a cytotoxic compound with an intracellular target. For identification of a putative transporter, the deletion library of non-essential transporters is treated with inhibitory concentrations of the compound and resistant strains are selected. These resistant strains probably lack the transporter responsible for the uptake of the tested compound. As exemplified, the deletion of transporter 2 interfered in the uptake of the xenobiotic and resulted in growth of this strain even in the presence of toxic concentrations of the tested molecule. As presented, transporter 2 is potentially responsible for the compound's uptake.

Figure 2. **Experimental pipeline.** Using the Synthetic Genetic Array methodology, a library of double-deletants of non-essential plasma membrane transporter encoding genes was constructed to allow the rapid identification of *kan*MX deletions by barcode sequencing. Once the sub-lethal doses of commercial xenobiotics were defined, two approaches were employed for import-route identification. A low-throughput screening in plate-based assay was performed for selection of strains resistant to compounds, followed by barcode sequencing for identification of the transporter-gene deletion responsible for the resistance phenotype. Chemical genomic profiling is a high-throughput approach employed to determine the relative abundance of transporter-gene deletion strains in the presence of a xenobiotic, and thus suggest putative

1030 importers and exporters. In both strategies, validation assays were conducted for
1031 confirmation of putative transport routes.

1032

1033 Figure 3. **Spot test for inhibitory concentration definition**. Serial dilutions (5x) of
1034 transporter-gene double- and single-mutant pool, wild type (BY4741) and isolated
1035 single-mutant *(trx2::kanMX* and *cpr1::kanMX) S. cerevisiae* strains spotted onto YNB+Sc
1036 plates containing the indicated concentrations of xenobiotics. For chlorothalonil,
1037 difenoconazole, epoxiconazole, fluconazole, ketoconazole, tebuconazole, 1,10-
1038 phenanthroline, captan, tamoxifen, and tunicamycin, it is possible to see that the
1039 double-mutant pool library presents more resistant strains than the single-mutant pool.
1040 For ammonium pyrrolidinedithiocarbamate, 3,4-dichloroisocoumarin, irgasan, and
1041 mancozeb, the single-mutant library presents more resistant strains, which may be due
1042 to the group of deletions not represented in the double gene-deletion library or because
1043 of the cell background. 5-fluorocytosine shows a very similar pattern in the two libraries
1044 and 8-hydroxyquinoline shows a pattern that seems to correspond to a cell background
1045 from the double-deletion library. Other compounds did not present a selective
1046 cytotoxicity between libraries.

1047

1048 Figure 4. **Selection of transporter-gene deletion strains resistant to xenobiotics.**
1049 Approximately 10^3 or 10^5 colony-forming units (CFUs) of wild type (BY4741) or
1050 transporter-gene deletion pool were plated onto YNB + Sc agar plates with the indicated

1051 concentrations of xenobiotics (or solvent control – DMSO 2%) to identify putative
1052 differences in number and size of drug-resistant colonies. Resistant transporter-gene
1053 deletion colonies were picked for barcode identification.

1054

1055 Figure 5. **Relative abundance of double-mutant library strains in the presence of**
1056 **cytotoxic concentrations of xenobiotics evaluated by CGP.** Resistant strains (log_2 fold
1057 change > 0) indicate the potential involvement of the protein encoded by the deleted
1058 gene in uptake of the xenobiotic (Importers). Sensitive strains (log_2 fold change < 0)
1059 indicate the potential involvement of the deleted gene's product in efflux of the
1060 xenobiotic (Exporters). Strains with the highest and lowest abundance were labeled for
1061 identification.

1062

1063 Figure 6. **Principal components analysis of all treatments from CGP performed with our**
1064 **transporter-gene double deletion library and sub lethal dose of xenobiotics.** Azole
1065 compounds group in the PCA plot, with exception of fluconazole. Agrochemical triazoles
1066 (difenoconazole, epoxiconazole and tebuconazole) and imidazoles (clotrimazole and
1067 ketoconazole) form two subgroups. This may indicate a similar strain composition profile
1068 and probably an involvement of a set of transporter proteins in the carriage of these
1069 compounds across the cell membrane.

1070

Figure 7. **Validation of double mutant resistance to 1,10-phenanthroline.** The panels present a spot-test of serial dilutions of double-deletion strains in the presence of 1,10-phenanthroline or 2% DMSO control. Combinations of mutations in genes encoding large molecule transporters (Arn1p, Arn2p, Enb1p or Fui1p) are resistant to the drug whereas single mutants *anr1*Δ, *arn2*Δ, *enb1*Δ or mutations in combination with the gene encoding iron permease Ftr1p do not confer a growth advantage.

Figure 8. **Relationship between azole influx and efflux transporters based on CGP results.** The analysis shows a good correlation ($r^2 > 0.95$) between proposed transport routes for agrochemical azoles (difenoconazole, epoxiconazole and tebuconazole) members of the 1,2,4 – triazole class and between the animal antifungals clotrimazole and ketoconazole ($r^2 = 0.9728$), which are members of imidazole class. A, B, C, D, E and F presents the correlation graphs with clotrimazole, difenoconazole, epoxiconazole, fluconazole, ketoconazole and tebuconazole, respectively, in abscissa and other 5 in ordinate. G presents the chemical structure of the azole xenobiotics. Different colors identify the xenobiotic represented. Strains with the highest and lowest abundance were labeled for identification.

Figure 9**. Evaluation of resistance or sensitivity phenotypes in double-deletion strains for putative importers and a known exporter of azoles compounds.** The panels present spot-test of serial dilutions of double-deletion strains in the presence of the 6 azoles compounds: clotrimazole, difenoconazole, epoxiconazole, fluconazole, ketoconazole

and tebuconazole. A. *itr1*Δ presented a resistance phenotype without the presence of a second transporter deletion and in the presence of Pdr5p. *pdr5*Δ, as expected, presented a sensitivity profile, confirming its importance in azole efflux. However, with the double mutant *itr1*Δ *pdr5*Δ, a sensitive phenotype is observed, indicating a secondary uptake route. *B. and C. itr2*Δ (*ITR1* paralog) and *nha1*Δ (experimental hit for azoles), respectively, were tested as a secondary route. Plate assays indicate that deletion of these transporters does not confer resistance and may indicate that they are not involved in the uptake.

Supplemental Materials

Table S1. Xenobiotics used in this study. Compound name, catalogue numbers and chemical properties.

Figure S1. Principal components analysis of all treatments from the CGP experiment, excluding fluconazole. Exclusion of fluconazole from PCA plot revealed a different profile for 5-fluorocytosine, the positive control of the assay. Azoles still group, with a clear separation of the subgroups triazoles and imidazoles.

Figure S2. High-density assay with 308 double-deletion strains (in quadruplicate) in the presence of inhibitory concentration of tunicamycin. Upper left panel shows a test plate

containing tunicamycin (4 days of growth). Upper right panel shows a control plate with DMSO 2% (4 days of growth). Middle panel presents a plate map (::*natMX* followed by ::*kanMX*) and the lower panel, the z-score for each quadruplicate. Green squares correspond to scores 3*SD and orange squares correspond to between 2 and 3*SD. High-density assay presents the same DMSO 2% plate as the experiment control.

Figure S3. High-density assay with 308 double-deletion strains (in quadruplicate) in the presence of inhibitory concentration of tamoxifen. Upper left panel shows a test plate containing tamoxifen (4 days of growth). Upper right panel shows a control plate with DMSO 2% (4 days of growth). Middle panel presents a plate map (::*natMX* followed by ::*kanMX*) and the lower panel, the z-score for each quadruplicate. Green squares correspond to scores 3*SD and orange squares correspond to between 2 and 3*SD. High-density assay presents the same DMSO 2% plate as the experiment control.

Figure S4. High-density assay with 308 double-deletion strains (in quadruplicate) in the presence of inhibitory concentration of difenoconazole. Upper left panel shows a test plate containing difenoconazole (4 days of growth). Upper right panel shows a control plate with DMSO 2% (4 days of growth). Middle panel presents a plate map (::*natMX* followed by ::*kanMX*) and the lower panel, the z-score for each quadruplicate. Green squares correspond to scores 3*SD and orange squares correspond to between 2 and 3*SD. High-density assay presents the same DMSO 2% plate as the experiment control.

Figure S5. High-density assay with 308 double-deletion strains (in quadruplicate) in the presence of inhibitory concentration of epoxiconazole. Upper left panel shows a test plate containing epoxiconazole (4 days of growth). Upper right panel shows a control plate with DMSO 2% (4 days of growth). Middle panel presents a plate map (::*natMX* followed by ::*kanMX*) and the lower panel, the z-score for each quadruplicate. Green squares correspond to scores 3*SD and orange squares correspond to between 2 and 3*SD. High-density assay presents the same DMSO 2% plate as the experiment control.

Figure S6. High-density assay with 308 double-deletion strains (in quadruplicate) in the presence of inhibitory concentration of tebuconazole. Upper left panel shows a test plate containing tebuconazole (4 days of growth). Upper right panel shows a control plate with DMSO 2% (4 days of growth). Middle panel presents a plate map (::*natMX* followed by ::*kanMX*) and the lower panel, the z-score for each quadruplicate. Green squares correspond to scores 3*SD and orange squares correspond to between 2 and 3*SD. High-density assay presents the same DMSO 2% plate as the experiment control.

Figure S7. High-density assay with 308 double-deletion strains (in quadruplicate) in the presence of inhibitory concentration of clotrimazole. Upper left panel shows a test plate containing clotrimazole (4 days of growth). Upper right panel shows a control plate with DMSO 2% (4 days of growth). Middle panel presents a plate map (::*natMX* followed by ::*kanMX*) and the lower panel, the z-score for each quadruplicate. Green squares

correspond to scores 3*SD and orange squares correspond to between 2 and 3*SD. High-density assay presents the same DMSO 2% plate as the experiment control.

Figure S8. High-density assay with 308 double-deletion strains (in quadruplicate) in the presence of inhibitory concentration of ketoconazole. Upper left panel shows a test plate containing ketoconazole (4 days of growth). Upper right panel shows a control plate with DMSO 2% (4 days of growth). Middle panel presents a plate map (::*natMX* followed by ::*kanMX*) and the lower panel, the z-score for each quadruplicate. Green squares correspond to scores 3*SD and orange squares correspond to between 2 and 3*SD. High-density assay presents the same DMSO 2% plate as the experiment control.

Data set S1. Differential abundance of barcodes between samples treated compared to untreated controls of 21 compounds. Each sheet corresponds to data from each compound, specified in the sheet name. Headlines are described on the first sheet (headlines meaning).

Tables

Table 1. **Transporter-gene deletion strains resistant to xenobiotics in agar plates (low-throughput) or liquid cultures (high-throughput).**

Compound	Low-Throughput Assay		High-Throughput Assay	
	[µM]	Hits	[µM]	Hits* (log_2 fold change)
5-Fluorocytosine	**8**	**7x *fcy2Δ,*** *ftr1Δ, tat2Δ*	**20**	*fui1Δ* (2.22), *tat1Δ* (1.23), *adp1Δ* (1.27), *bap3Δ* (0.93), ***fcy2Δ* (8.44),** *azr1Δ* (1.06), *gal2Δ* (0.59), *atr2Δ* (0.96), *nrt1Δ* (1.24), *pdr12Δ* (1.84), *ssu1Δ* (2.68), *aqy1Δ* (1.14)
Clotrimazole	**10**	*fui1Δ, mal31Δ, tpo2Δ, cch1Δ, mal11Δ, arn2Δ,* 2x *hxt1Δ, opt1Δ,* **4x *nha1Δ,*** *mep2Δ, lyp1Δ, alp1Δ, thi72Δ, pma2Δ*	**2**	***nha1Δ* (0.72)**
Ketoconazole	**25**	*gnp1Δ, mep1Δ, tok1Δ, jen1Δ,* **14x *nha1Δ***	**10**	*adp1Δ* (0.56), ***nha1Δ* (1.10)**
Difenoconazole Pestanal ®	**20**	*dtr1Δ, snq2Δ,* ***itr1Δ,*** *gnp1Δ,* ***tna1Δ,*** *arn1Δ, arn2Δ, gap1Δ,* **6x *nha1Δ,*** *mmt1Δ*	**0.16**	*adp1Δ* (0.70), ***itr1Δ* (0.90)**, *ftr1Δ* (1.08), ***tna1Δ* (0.63)**, *yor1Δ* (0.81), *tpo5Δ* (1.35), *tpo1Δ* (0.91), ***nha1Δ* (2.51)**, *smf1Δ* (0.93), *tpo4Δ* (0.73)
Epoxiconazole Pestanal ®	**0.8**	*pho89Δ,* 2x *hxt3Δ, ato3Δ,* **2x *itr1Δ,*** 2x *cch1Δ, dur3Δ, hxt5Δ, nft1Δ,* ***ybt1Δ,*** *mmt1Δ, mch5Δ, pma2Δ, aqy1Δ*	**0.032**	*adp1Δ* (0.75), *snq2Δ* (1.12), ***itr1Δ* (1.52),** *ftr1Δ* (1.94), *tna1Δ* (0.67), *yor1Δ* (0.97), *gef1Δ* (0.69), *tpo5Δ* (1.96), *tpo1Δ* (1.11), ***ybt1Δ* (0.61),** *nha1Δ* (3.93), *smf1Δ* (1.51), *tpo4Δ* (0.76), *dip5Δ* (0.67), *ctr1Δ* (0.76)
Tebuconazole Pestanal ®	**20**	*bap3Δ,* **2x *itr1Δ,*** *agp3Δ, hnm1Δ,* 2x *mep1Δ, hxt8Δ, nft1Δ, prm6Δ, atr1Δ, fet4Δ,* ***tpo4Δ,*** *mch5Δ, pma2Δ, aqy1Δ*	**0.32**	*adp1Δ* (0.69), ***itr1Δ* (1.04)**, *ftr1Δ* (0.94), *tna1Δ* (0.82), *yor1Δ* (0.81), *tpo5Δ* (1.19), *tpo1Δ* (0.73), *nha1Δ* (2.67), *smf1Δ* (0.84), ***tpo4Δ* (0.53)**, *ctr1Δ* (0.65)
Fluconazole	**100**	**3x *qdr3Δ, tat1Δ,*** *agp1Δ,* ***ady2Δ, adp1Δ, yor1Δ, arn1Δ, hxt4Δ,*** *gex2Δ,* ***bor1Δ, hol1Δ,*** *enb1Δ, nrt1Δ, ssu1Δ, aqy1Δ*	**75**	*seo1Δ* (1.60), *flr1Δ* (1.83), ***qdr3Δ* (2.72),** *bap2Δ* (2.57), ***tat1Δ* (2.66),** *pca1Δ* (1.76), *pho89Δ* (1.50), *mal31Δ* (2.57), ***ady2Δ* (1.73), *adp1Δ* (2.48),** *git1Δ* (1.66), *sit1Δ* (1.62), ***yor1Δ* (2.54), *arn1Δ* (1.98), *hxt4Δ* (2.79),** *hxt1Δ* (2.68), *hxt5Δ* (2.39), *qdr2Δ* (5.96), ***bor1Δ* (1.17), *hol1Δ* (5.57),** *mch5Δ* (1.54)
1,10-Phenanthroline	**35**	2x *fui1Δ, adp1Δ, itr1Δ, fcy2Δ, tpo2Δ, arn1Δ, arn2Δ, tok1Δ, mid1Δ, enb1Δ, pdr5Δ*	**10**	No hits
3,4-Dichloroisocoumarin	**16**	*itr1Δ,* YFL040WΔ, *hxt1Δ, kch1Δ, mmp1Δ, prm6Δ, lyp1Δ,* 2x	**10**	No hits

		*thi72*Δ, 2x *ssu1*Δ, *dip5*Δ		
8-Hydroxyquinoline	**7, 25, 50**	*pca1*Δ, 2x *fen2*Δ, *sit1*Δ, *ftr1*Δ, *mep1*Δ, 2x *arn2*Δ, *qdr1*Δ, *2x dal5*Δ, *hol1*Δ, *aus1*Δ	**50**	*ctr1*Δ (1.35)
Ammonium pyrrolidinedithiocarbamate	**4**	*dtr1*Δ, *zrt1*Δ, *pdr11*Δ, *itr2*Δ	N.P.	
Artesunate	**400**	2x *flr1*Δ, 2x *can1*Δ, YFL040WΔ, *alr2*Δ, *agp3*Δ, *arn1*Δ, *hxt4*Δ, ***tpo1*Δ,** *ybt1*Δ, *atr2*Δ, *bor1*Δ	**200**	*tna1*Δ (0.79), ***tpo1*Δ (0.72),** *nha1*Δ (0.91), *hxt17*Δ (0.72)
Cantharidin	**60**	2x *pca1*Δ, *fen2*Δ, *zrt1*Δ, *yor1*Δ, *dur3*Δ, 2x *hxt1*Δ, *pdr11*Δ, *qdr1*Δ, *trk1*Δ, *hxt14*Δ, *itr2*Δ, *tpo4*Δ	N.P.	
Captan Pestanal ®	**5**	*dtr1*Δ, *bap3*Δ, *fcy2*Δ, *kch1*Δ, *jen1*Δ, *prm6*Δ, *mid1*Δ, *tpo4*Δ, *mch5*Δ, *put4*Δ, *sam3*Δ, *sge1*Δ	**1.6**	No hits
Carbendazim	**150, 200**	*agp1*Δ, *ady2*Δ, *adp1*Δ, *ato3*Δ, ***tna1*Δ**, *yor1*Δ, *pdr11*Δ, *kch1*Δ**,** ***nft1*Δ**, *ybt1*Δ, ***nha1*Δ**, *atr1*Δ, *hxt14*Δ, ***pdr5*Δ**	**200**	*fur4*Δ (0.77), *tat1*Δ (1.77), *cin10*Δ (0.99), *hnm1*Δ (0.55), ***tna1*Δ (2.01), *nft1*Δ (0.77), *nha1*Δ (2.04),** *aqr1*Δ (0.53), *tat2*Δ (1.08), ***pdr5*Δ (1.29),** *ctr1*Δ (0.99)
Chlorothalonil Pestanal ®	**0.1, 1**	*fur4*Δ, *hxt3*Δ, *ato3*Δ, *gnp1*Δ, 4x *zrt1*Δ, *nft1*Δ, *sul2*Δ, ***atr1*Δ**, *bor1*Δ, *bio5*Δ, *pdr5*Δ, *mch5*Δ, *dip5*Δ	**0.8**	***atr1*Δ (0.77)**
Dazomet Pestanal ®	**15, 20**	3x YDL199CΔ, *gex2*Δ, *mep2*Δ, *smf1*Δ, *ssu1*Δ, *tpo3*Δ	N.P.	
Iprobenfos Pestanal ®	**200**	*flr1*Δ, *qdr3*Δ, *git1*Δ, *hxt10*Δ, *mal11*Δ, *sul2*Δ, *hxt2*Δ, *aus1*Δ, *thi72*Δ, *tpo4*Δ, *put4*Δ, *ssu1*Δ, *aqy1*Δ	**200**	No hits
Irgasan	**40, 50**	*pca1*Δ, *stl1*Δ, *alr2*Δ, *trk1*Δ, *aqr1*Δ, 2x *mep2*Δ, *lyp1*Δ, 2x *mid1*Δ, *ato2*Δ, 2x *aus1*Δ, *sam3*Δ	**15**	*fen2*Δ (1.94), *arn1*Δ (0.52), *arn2*Δ (0.69)
Mancozeb Pestanal ®	**10, 20, 30**	*sul1*Δ, *stl1*Δ, *zrt1*Δ, *opt1*Δ, *nha1*Δ, *atr1*Δ	N.P.	
N-Phenylanthranilic Acid	-	no resistant selected	**100**	*snq2*Δ (0.68), *tna1*Δ (0.87), *mid1*Δ (0.76), *pdr5*Δ (1.01)
Tamoxifen	**365**	YDL199CΔ, *opt1*Δ, *kch1*Δ, *dal5*Δ, 7x *tpo5*Δ, 3x *nha1*Δ, *atr1*Δ, *mep2*Δ, *itr2*Δ, *mch5*Δ	**40**	*adp1*Δ (0.50), *tna1*Δ (1.18)
Tunicamycin	**4**	*fui1*Δ, *flr1*Δ, 11x *fur4*Δ, *qdr3*Δ, *mal31*Δ, *zrt1*Δ, *nft1*Δ, *tpo4*Δ, *aqy1*Δ	**1**	No hits

1175 * $\log_2$ fold change≥0.5; p-value adjusted for multiple tests (padj) ≤ 0.1; p-value ≤ 0.001.
1176 N.P. indicate assays not performed. Bold deletant names correspond to those that are
1177 repeated between low- and high-throughput screenings.
1178
1179
1180
1181
1182
1183
1184
1185
1186
1187
1188

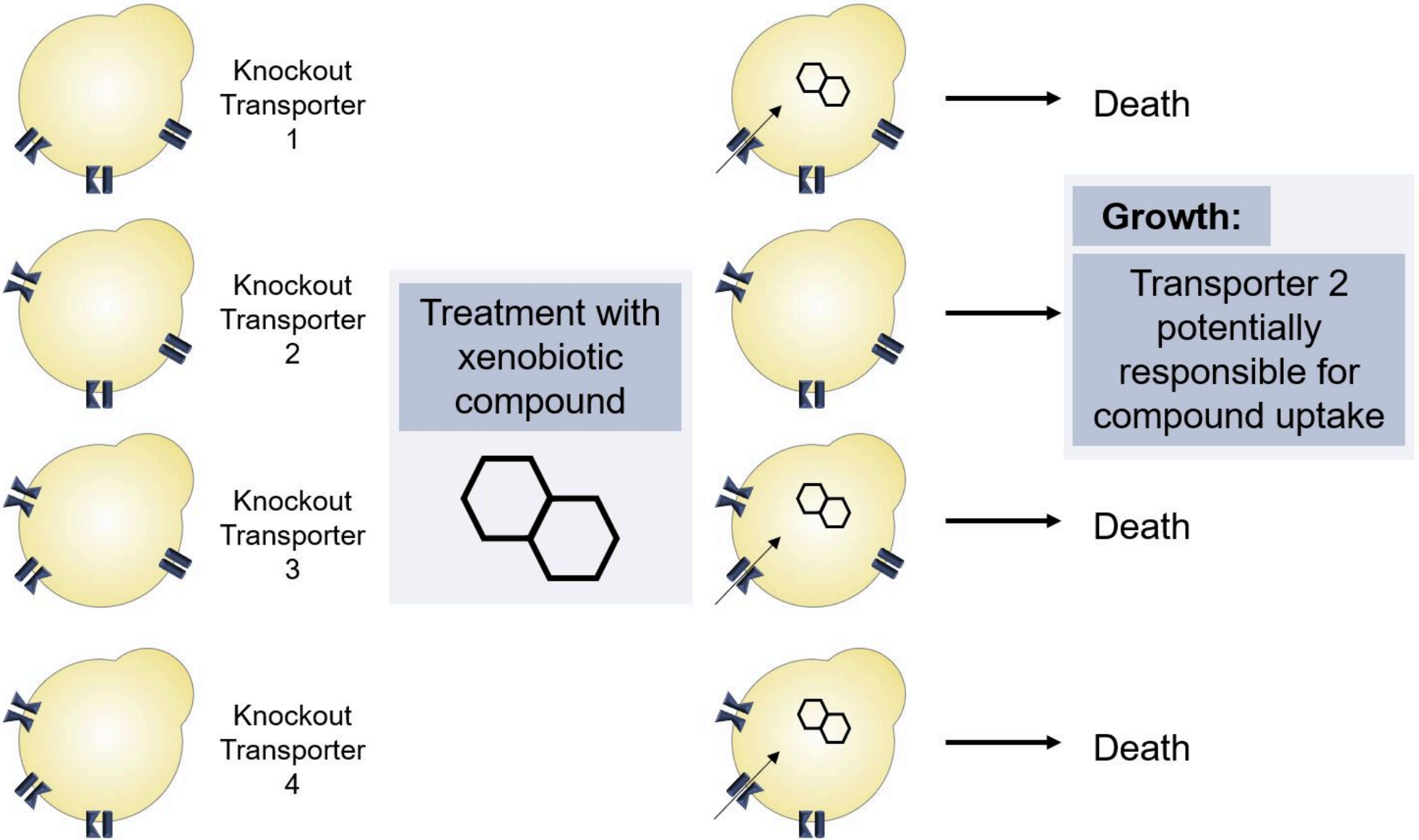
Knockout Transporter 1
Knockout Transporter 2
Knockout Transporter 3
Knockout Transporter 4
Treatment with xenobiotic compound
Death
Growth:
Transporter 2 potentially responsible for compound uptake
Death
Death

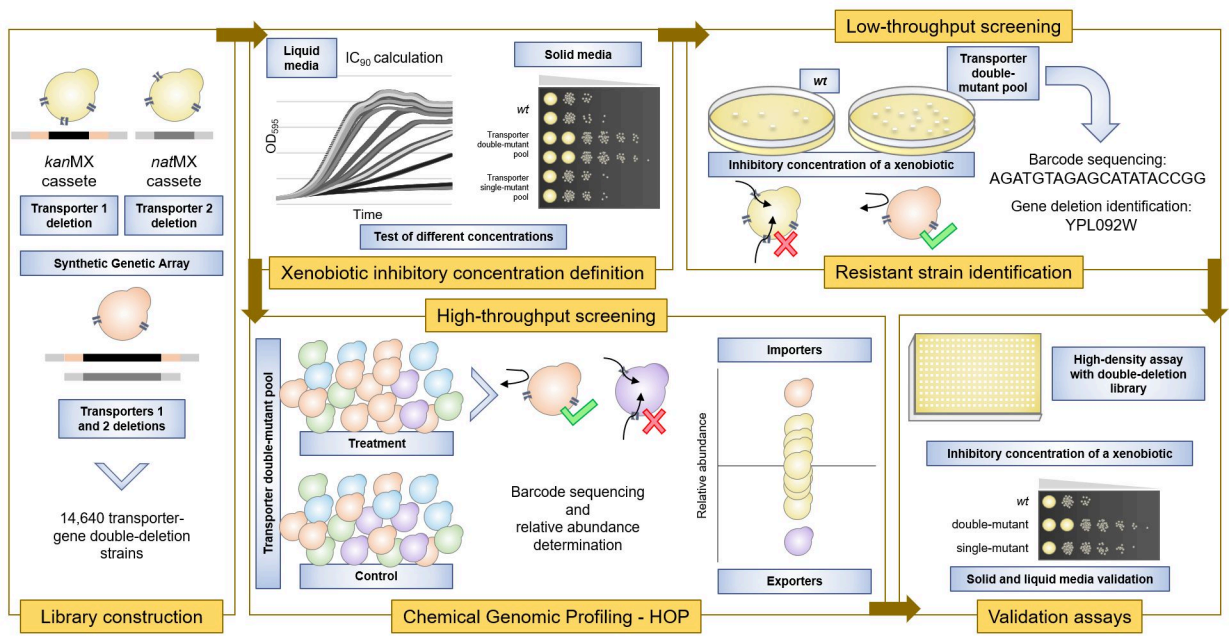
kanMX cassete
natMX cassete
Transporter 1 deletion
Transporter 2 deletion
Synthetic Genetic Array
Transporters 1 and 2 deletions
14,640 transporter-gene double-deletion strains
Library construction
Liquid media
IC90 calculation
OD595
Time
Solid media
wt
Transporter double-mutant pool
Transporter single-mutant pool
Test of different concentrations
Xenobiotic inhibitory concentration definition
Low-throughput screening
wt
Transporter double-mutant pool
Inhibitory concentration of a xenobiotic
Barcode sequencing: AGATGTAGAGCATATACCGG
Gene deletion identification: YPL092W
Resistant strain identification
High-throughput screening
Transporter double-mutant pool
Treatment
Control
Barcode sequencing and relative abundance determination
Importers
Relative abundance
Exporters
Chemical Genomic Profiling - HOP
High-density assay with double-deletion library
Inhibitory concentration of a xenobiotic
wt
double-mutant
single-mutant
Solid and liquid media validation
Validation assays

Strains
BY4741
Transporter double-mutant pool
Transporter single-mutant pool
*trx2*Δ::*kan*MX
*cpr1*Δ::*kan*MX

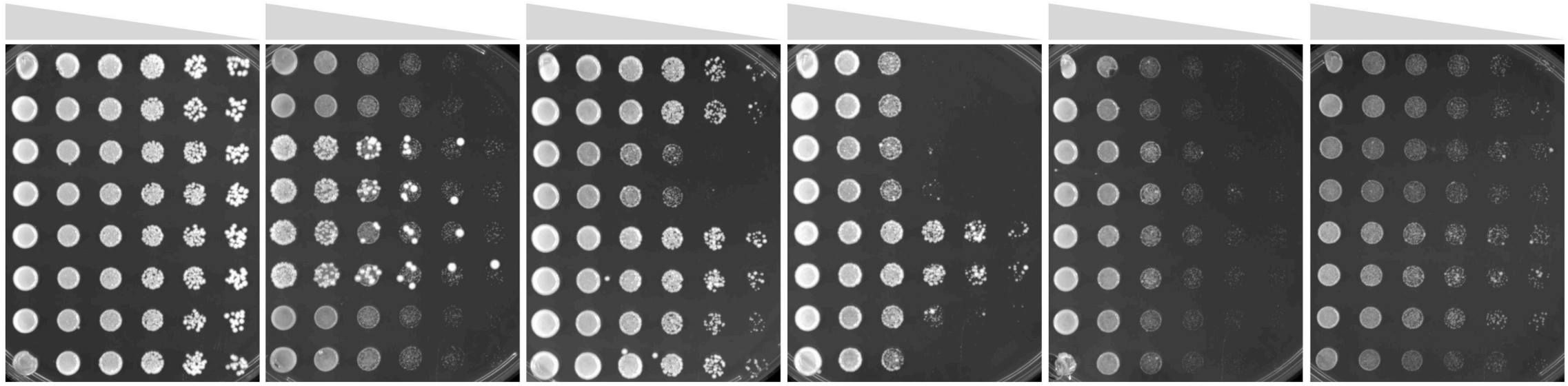

DMSO 2%
5-Fluorocytosine 40 µM
8-Hydroxyquinoline 50 µM
Ammonium pyrrolidinedithiocarbamate 10 µM
Artesunate 400 µM
Cantharidin 100 µM

Strains
BY4741
Transporter double-mutant pool
Transporter single-mutant pool
*trx2*Δ::*kan*MX
*cpr1*Δ::*kan*MX

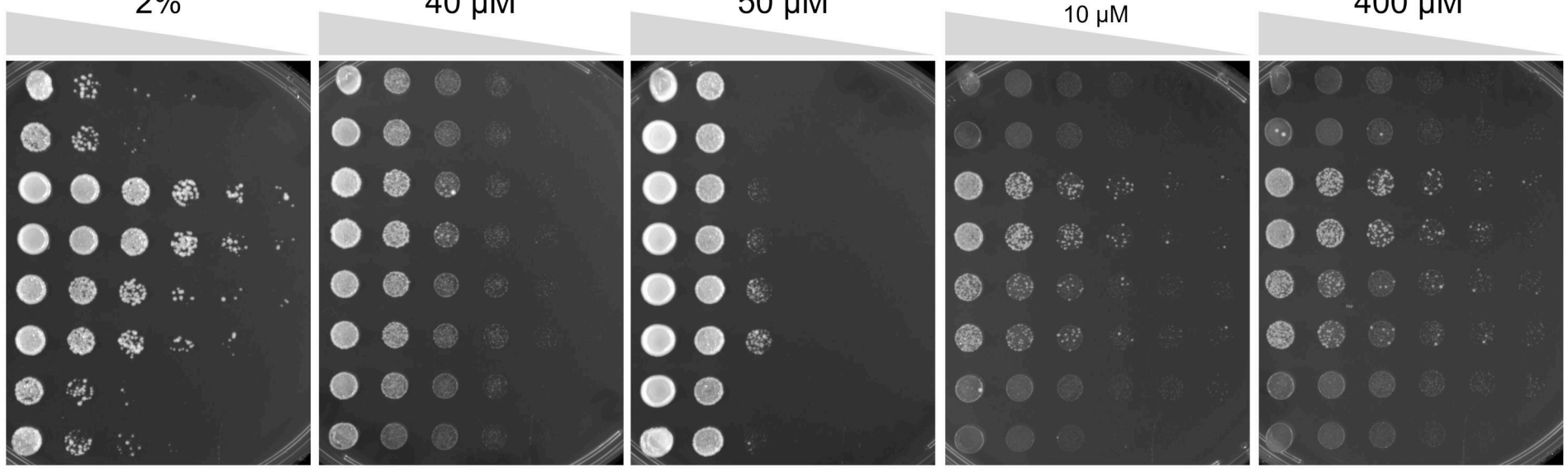

Chlorothalonil 1 µM
Clotrimazole 5 µM
Dazomet 20 µM
Difenoconazole 4 µM
Epoxiconazole 0.8 µM

Strains
BY4741
Transporter double-mutant pool
Transporter single-mutant pool
*trx2*Δ::*kan*MX
*cpr1*Δ::*kan*MX

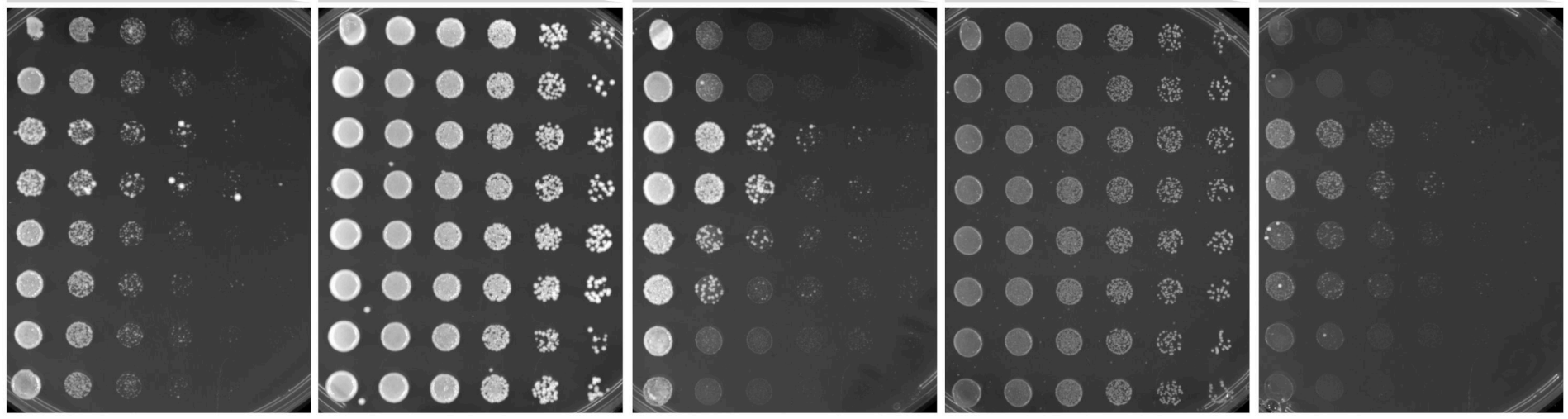

Fluconazole 100 µM
Iprobenfos 200 µM
Ketoconazole 20 µM
N-Phenylanthranilic Acid 200 µM
Tebuconazole 20 µM

Strains
BY4741
Transporter double-mutant pool
Transporter single-mutant pool
*trx2*Δ::*kan*MX
*cpr1*Δ::*kan*MX

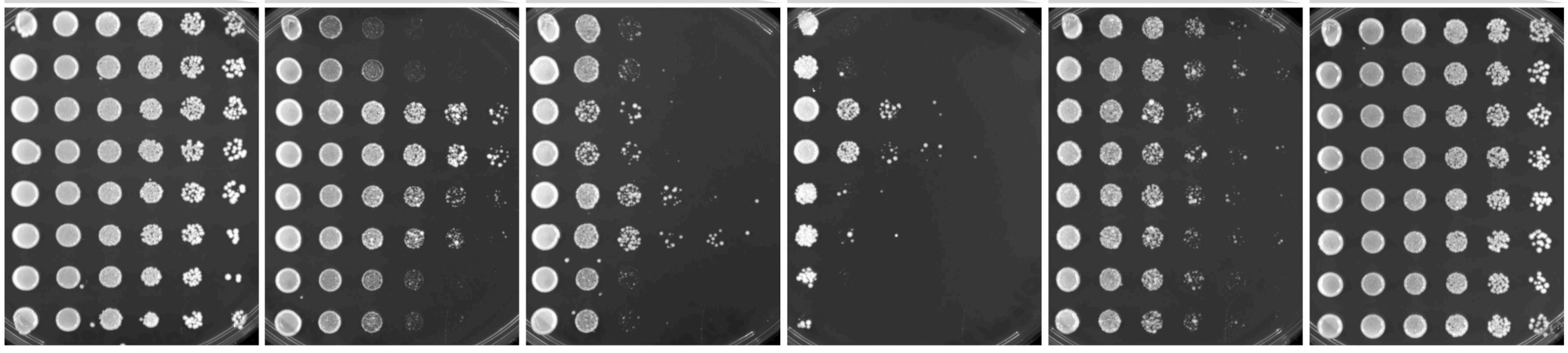

DMSO 2%
1,10-Phenanthroline 14 µM
3,4-Dichloroisocoumarin 32 µM
Captan 5 µM
Carbendazim 150 µM
Cisplatin 200 µM

Strains
BY4741
Transporter double-mutant pool
Transporter single-mutant pool
*trx2*Δ::*kan*MX
*cpr1*Δ::*kan*MX

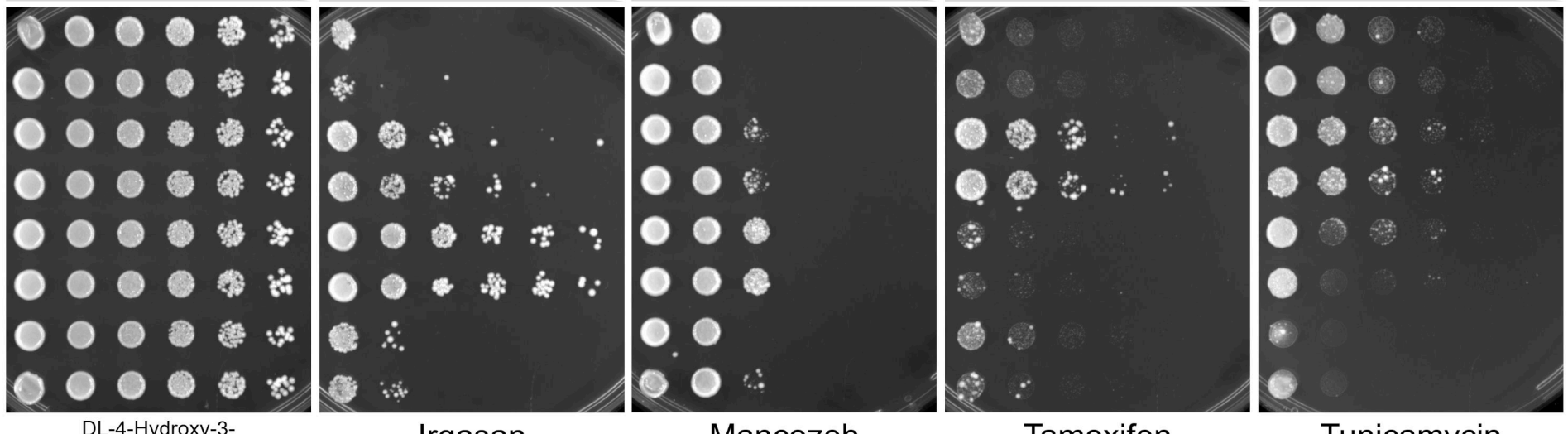

DL-4-Hydroxy-3-Methoxymandelic Acid 800 µM
Irgasan 22.5 µM
Mancozeb 30 µM
Tamoxifen 182.5 µM
Tunicamycin 2 µM

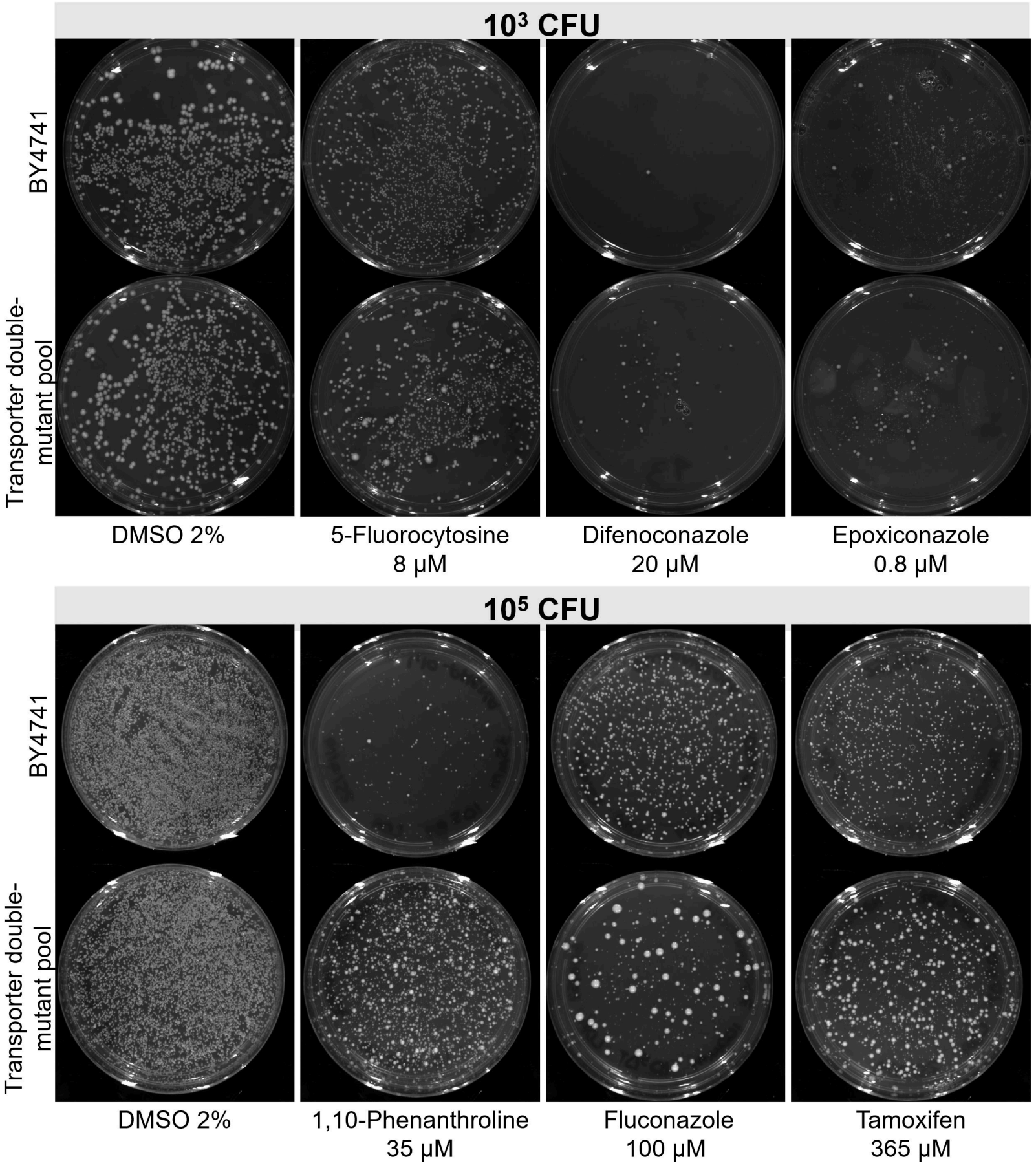
10³ CFU
BY4741
Transporter double-mutant pool
DMSO 2%
5-Fluorocytosine 8 µM
Difenoconazole 20 µM
Epoxiconazole 0.8 µM
10⁵ CFU
BY4741
Transporter double-mutant pool
DMSO 2%
1,10-Phenanthroline 35 µM
Fluconazole 100 µM
Tamoxifen 365 µM

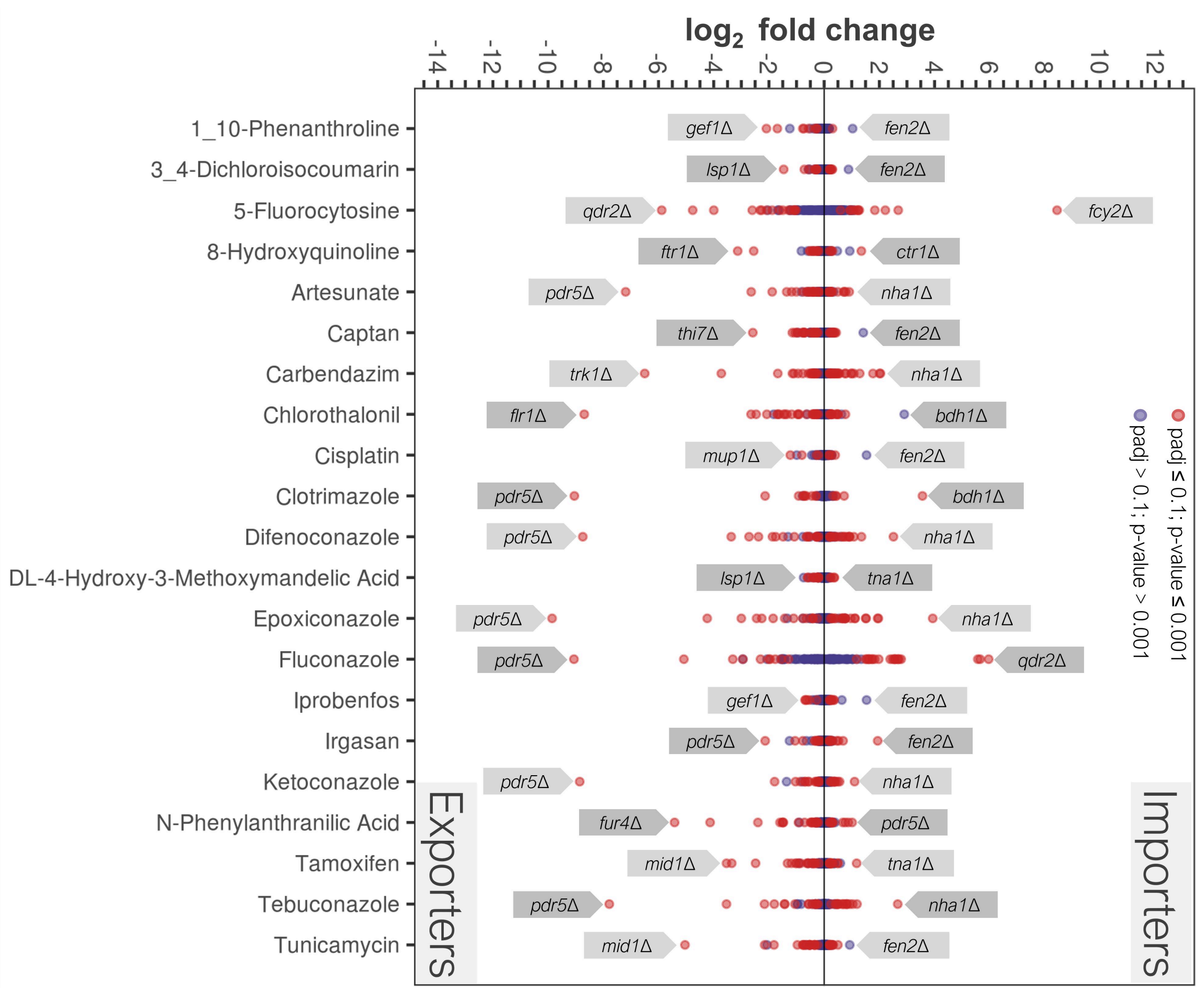
log2 fold change
-14
-12
-10
-8
-6
-4
-2
0
2
4
6
8
10
12
1_10-Phenanthroline
3_4-Dichloroisocoumarin
5-Fluorocytosine
8-Hydroxyquinoline
Artesunate
Captan
Carbendazim
Chlorothalonil
Cisplatin
Clotrimazole
Difenoconazole
DL-4-Hydroxy-3-Methoxymandelic Acid
Epoxiconazole
Fluconazole
Iprobenfos
Irgasan
Ketoconazole
N-Phenylanthranilic Acid
Tamoxifen
Tebuconazole
Tunicamycin
gef1Δ
fen2Δ
lsp1Δ
fen2Δ
qdr2Δ
fcy2Δ
ftr1Δ
ctr1Δ
pdr5Δ
nha1Δ
thi7Δ
fen2Δ
trk1Δ
nha1Δ
flr1Δ
bdh1Δ
mup1Δ
fen2Δ
pdr5Δ
bdh1Δ
pdr5Δ
nha1Δ
lsp1Δ
tna1Δ
pdr5Δ
nha1Δ
pdr5Δ
qdr2Δ
gef1Δ
fen2Δ
pdr5Δ
fen2Δ
pdr5Δ
nha1Δ
fur4Δ
pdr5Δ
mid1Δ
tna1Δ
pdr5Δ
nha1Δ
mid1Δ
fen2Δ
padj ≤ 0.1; p-value ≤ 0.001
padj > 0.1; p-value > 0.001
Exporters
Importers

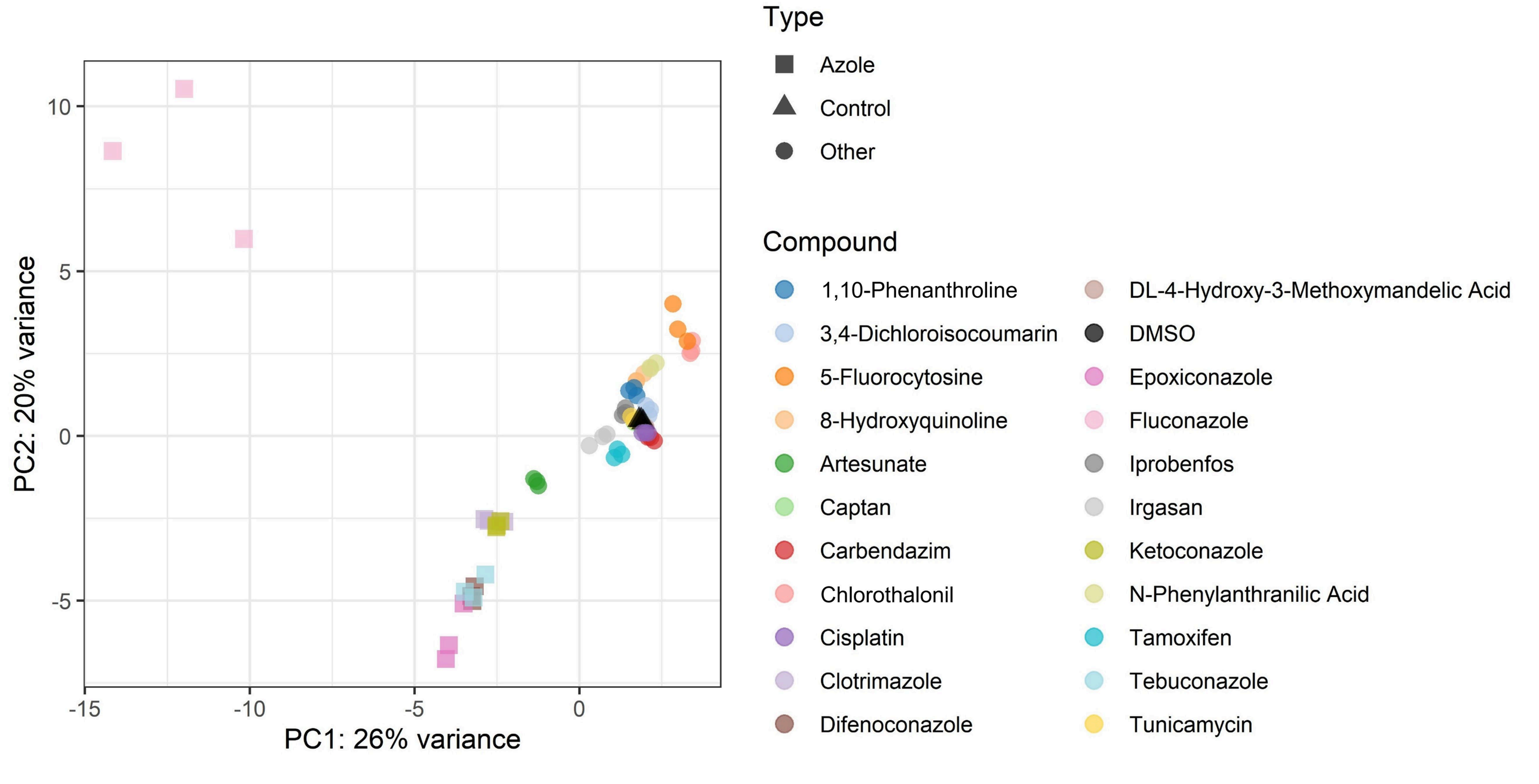
PC2: 20% variance
PC1: 26% variance
10
5
0
-5
-15
-10
-5
0
Type
Azole
Control
Other
Compound
1,10-Phenanthroline
3,4-Dichloroisocoumarin
5-Fluorocytosine
8-Hydroxyquinoline
Artesunate
Captan
Carbendazim
Chlorothalonil
Cisplatin
Clotrimazole
Difenoconazole
DL-4-Hydroxy-3-Methoxymandelic Acid
DMSO
Epoxiconazole
Fluconazole
Iprobenfos
Irgasan
Ketoconazole
N-Phenylanthranilic Acid
Tamoxifen
Tebuconazole
Tunicamycin

Column 1		Column 4	
***::nat*MX**	***::kan*MX**	***::nat*MX**	***::kan*MX**
arn1Δ	*fui1Δ*	*fui1Δ*	*ftr1Δ*
arn2Δ	*fui1Δ*	*arn1Δ*	*ftr1Δ*
enb1Δ	*fui1Δ*	*arn2Δ*	*ftr1Δ*
arn2Δ	*arn1Δ*	*enb1Δ*	*ftr1Δ*
enb1Δ	*arn1Δ*	-	*fui1Δ*
enb1Δ	*arn2Δ*	-	*arn1Δ*
BY4741		-	*arn2Δ*
-	*ftr1Δ*	-	*enb1Δ*

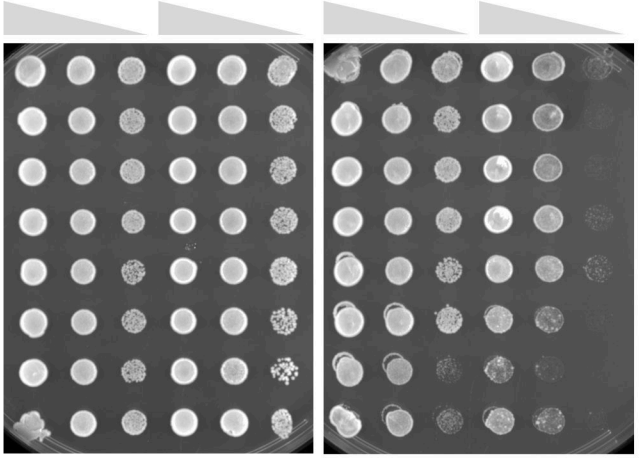

DMSO 2%

1,10-Phenanthroline 14 µM

A.

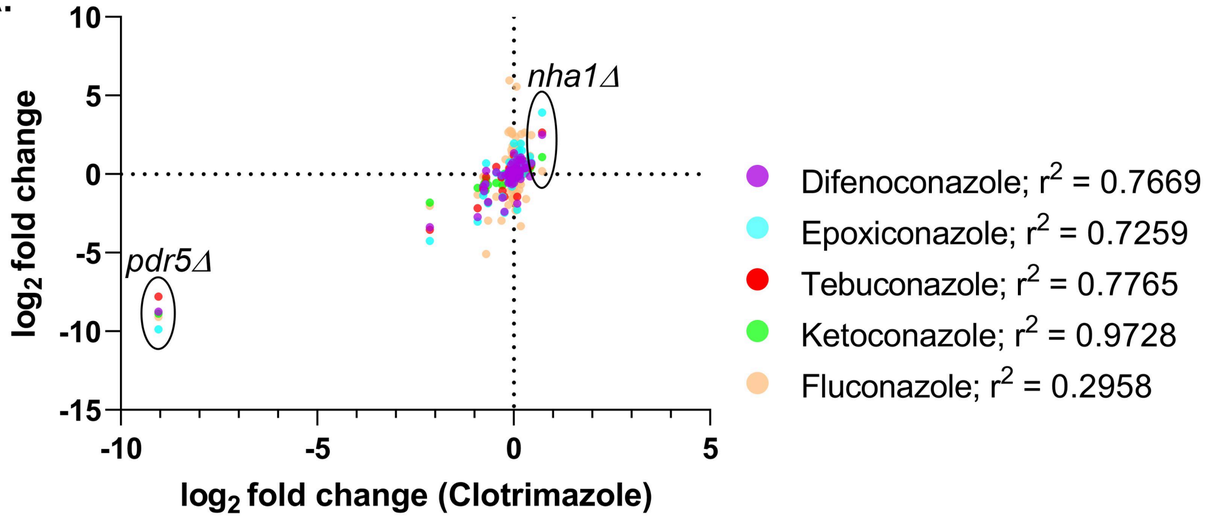
nha1Δ
pdr5Δ
log2 fold change
log2 fold change (Clotrimazole)
Difenoconazole; r2 = 0.7669
Epoxiconazole; r2 = 0.7259
Tebuconazole; r2 = 0.7765
Ketoconazole; r2 = 0.9728
Fluconazole; r2 = 0.2958

B.

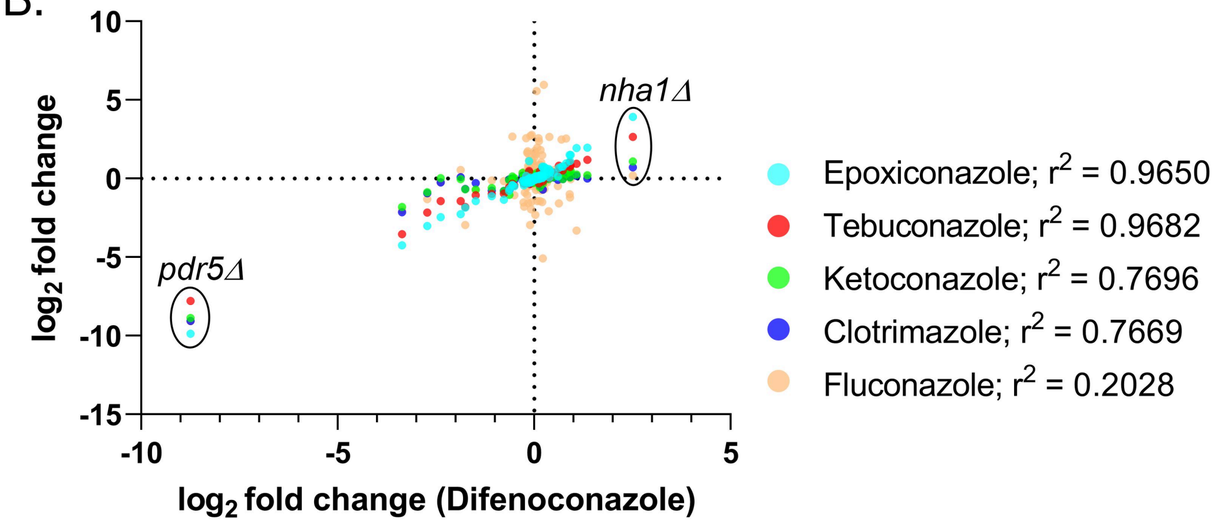
nha1Δ
pdr5Δ
log2 fold change
log2 fold change (Difenoconazole)
Epoxiconazole; r2 = 0.9650
Tebuconazole; r2 = 0.9682
Ketoconazole; r2 = 0.7696
Clotrimazole; r2 = 0.7669
Fluconazole; r2 = 0.2028

C.

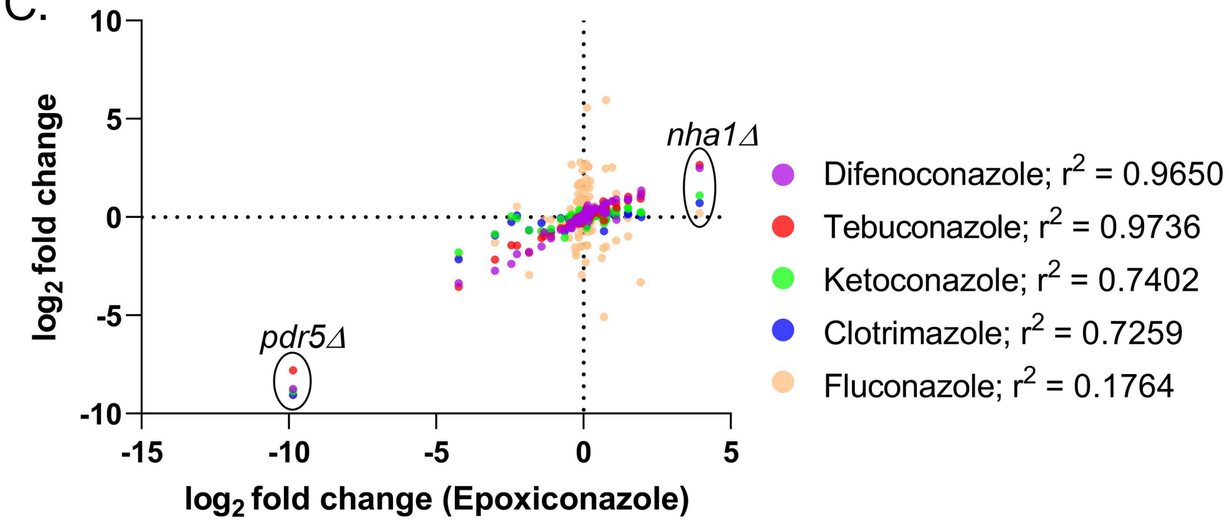
nha1Δ
pdr5Δ
log2 fold change
log2 fold change (Epoxiconazole)
Difenoconazole; r2 = 0.9650
Tebuconazole; r2 = 0.9736
Ketoconazole; r2 = 0.7402
Clotrimazole; r2 = 0.7259
Fluconazole; r2 = 0.1764

D.

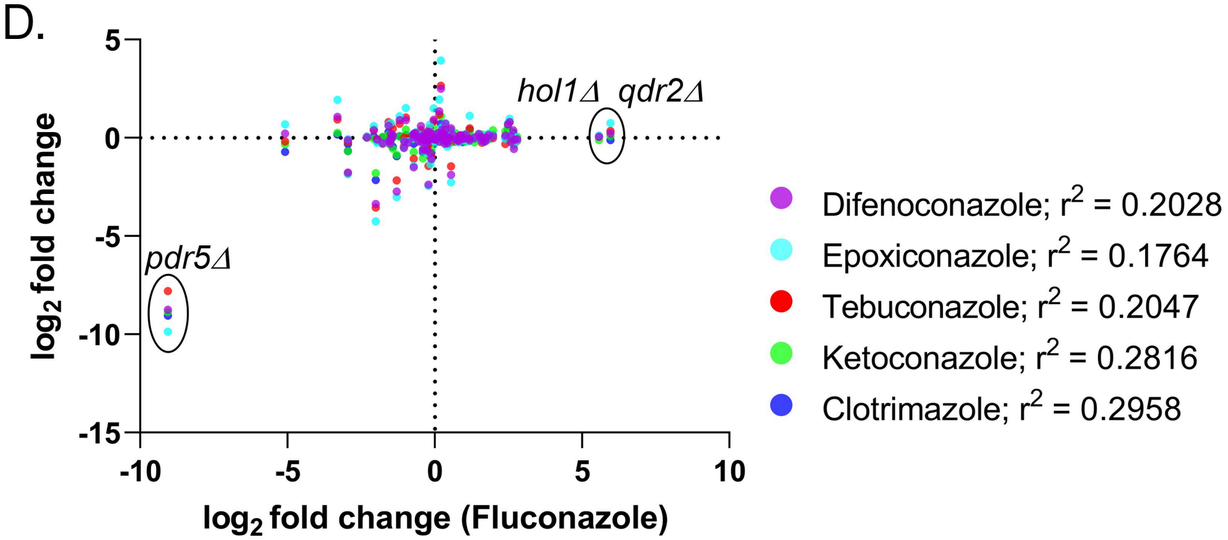
hol1Δ qdr2Δ
pdr5Δ
log2 fold change
log2 fold change (Fluconazole)
Difenoconazole; r2 = 0.2028
Epoxiconazole; r2 = 0.1764
Tebuconazole; r2 = 0.2047
Ketoconazole; r2 = 0.2816
Clotrimazole; r2 = 0.2958

E.

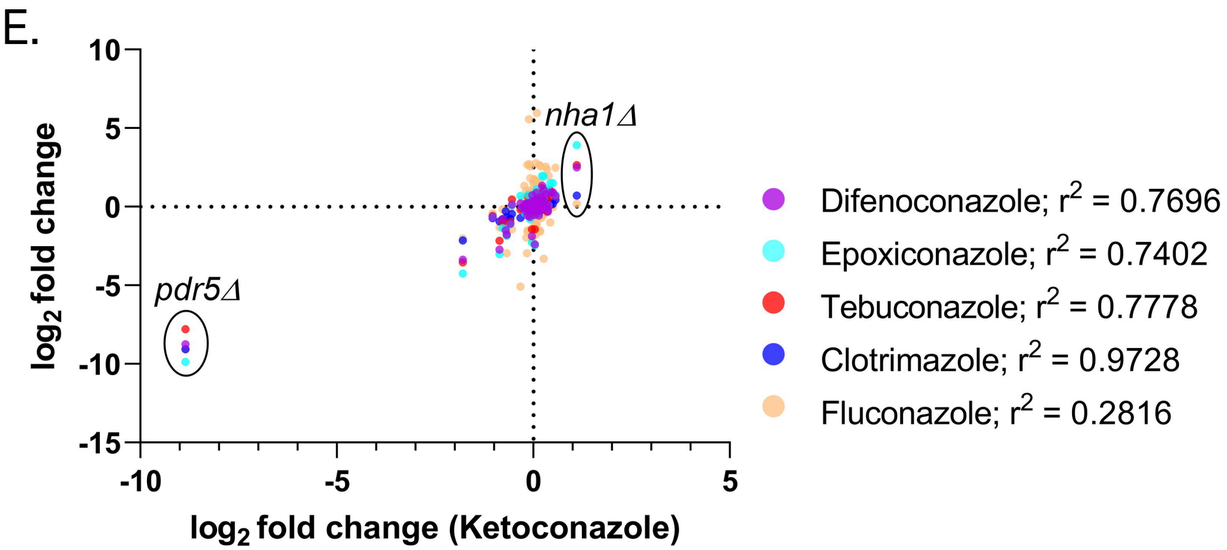
nha1Δ
pdr5Δ
log2 fold change
log2 fold change (Ketoconazole)
Difenoconazole; r2 = 0.7696
Epoxiconazole; r2 = 0.7402
Tebuconazole; r2 = 0.7778
Clotrimazole; r2 = 0.9728
Fluconazole; r2 = 0.2816

F.

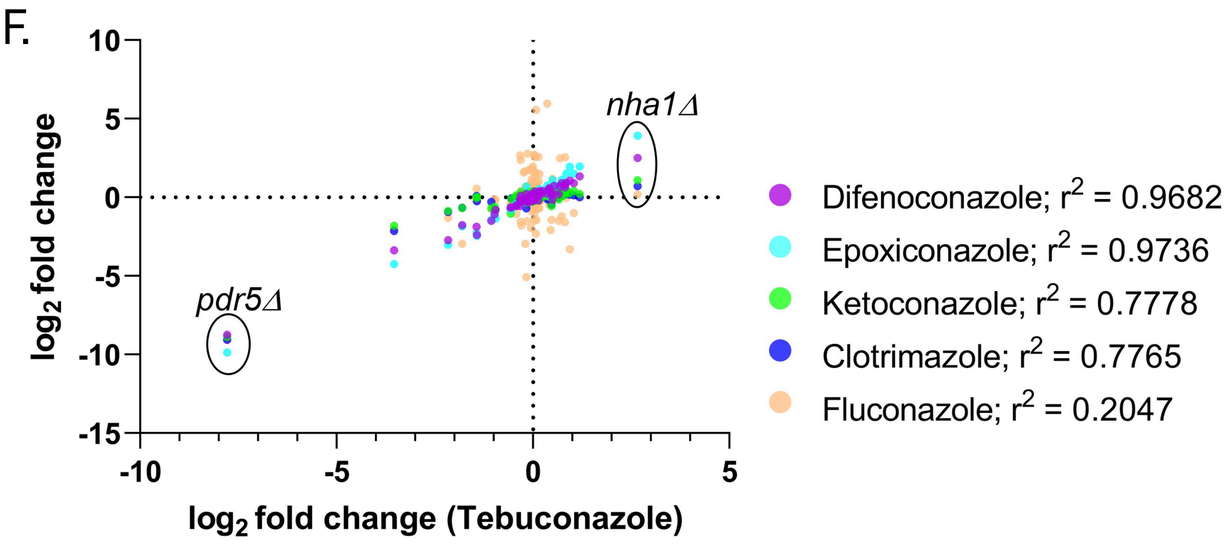
nha1Δ
pdr5Δ
log2 fold change
log2 fold change (Tebuconazole)
Difenoconazole; r2 = 0.9682
Epoxiconazole; r2 = 0.9736
Ketoconazole; r2 = 0.7778
Clotrimazole; r2 = 0.7765
Fluconazole; r2 = 0.2047

G.

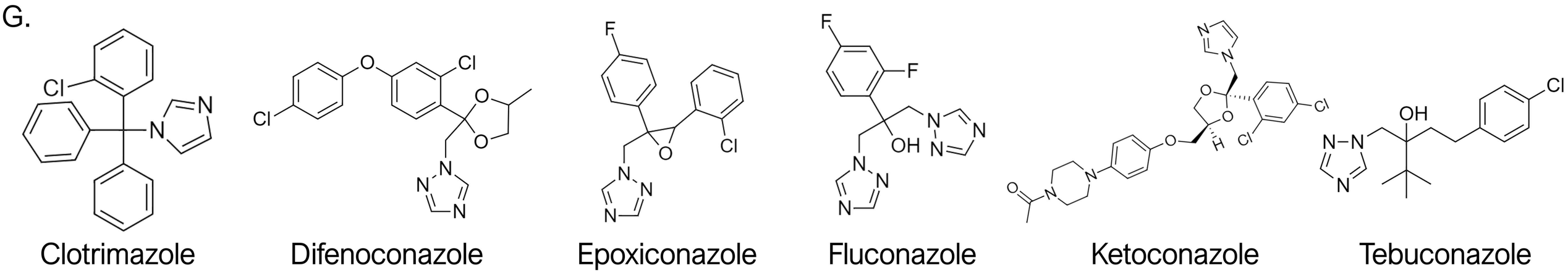
Clotrimazole
Difenoconazole
Epoxiconazole
Fluconazole
Ketoconazole
Tebuconazole

A.

::natMX	::kanMX
itr1Δ	his3Δ
pdr5Δ	his3Δ
itr1Δ	pdr5Δ
pdr5Δ	itr1Δ
fcy2Δ	his3Δ
BY4741	

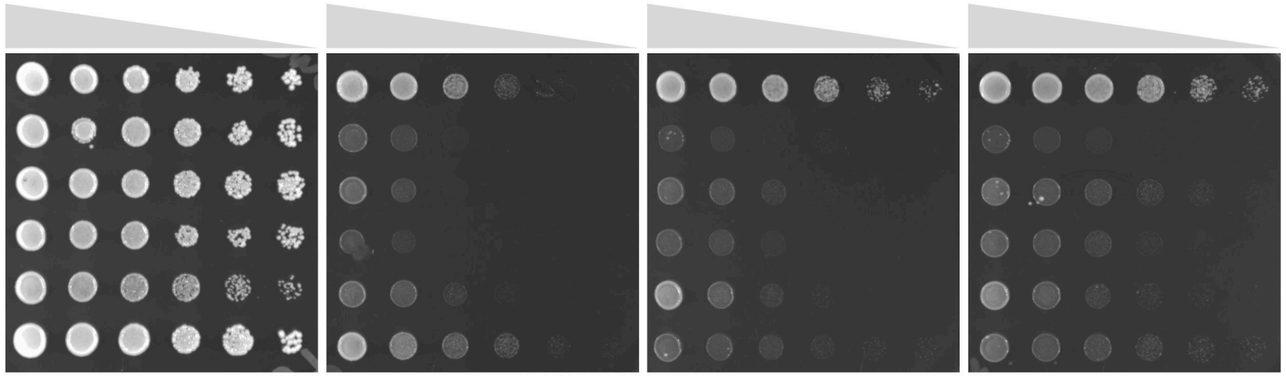

DMSO 1.5 % | Clotrimazole 5 µM | Difenoconazole 4 µM | Epoxiconazole 0.8 µM

itr1Δ	his3Δ
pdr5Δ	his3Δ
itr1Δ	pdr5Δ
pdr5Δ	itr1Δ
fcy2Δ	his3Δ
BY4741	

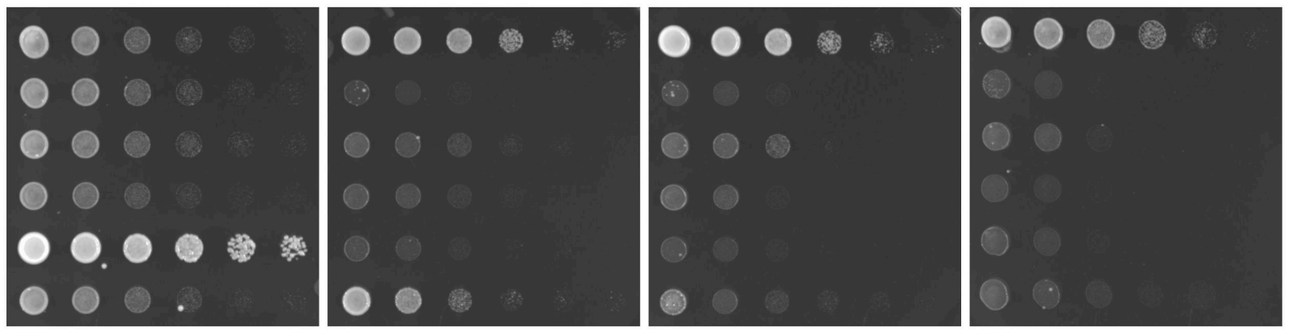

5-Fluorocytosine 40 µM | Fluconazole 150 µM | Ketoconazole 20 µM | Tebuconazole 20 µM

Growth

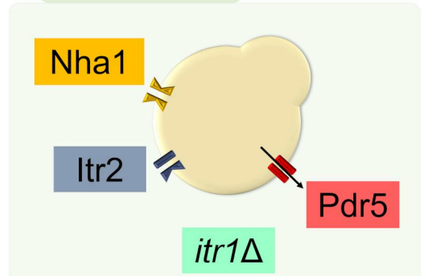

Little growth or death

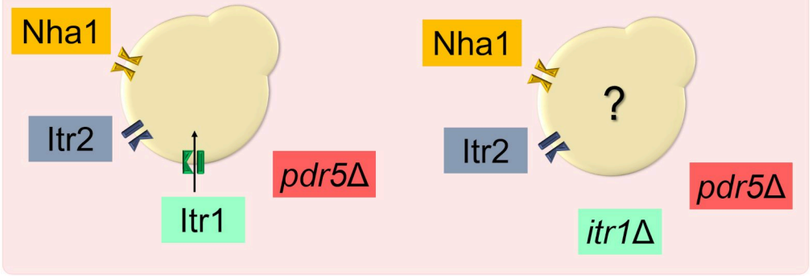

B.

::natMX	::kanMX
itr1Δ	his3Δ
itr2Δ	his3Δ
itr1Δ	itr2Δ
itr2Δ	itr1Δ
fcy2Δ	his3Δ
BY4741	

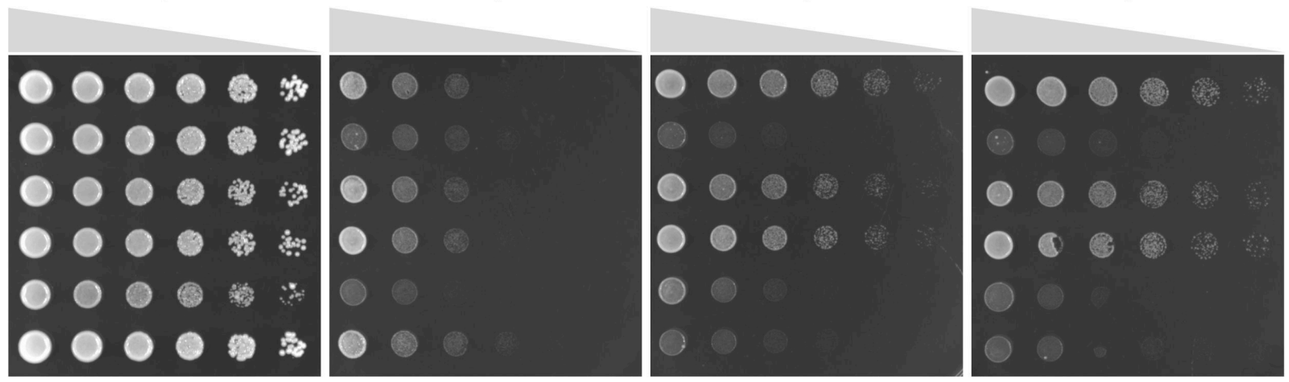

DMSO 1.5 % | Clotrimazole 5 µM | Difenoconazole 4 µM | Epoxiconazole 0.8 µM

itr1Δ	his3Δ
itr2Δ	his3Δ
itr1Δ	itr2Δ
itr2Δ	itr1Δ
fcy2Δ	his3Δ
BY4741	

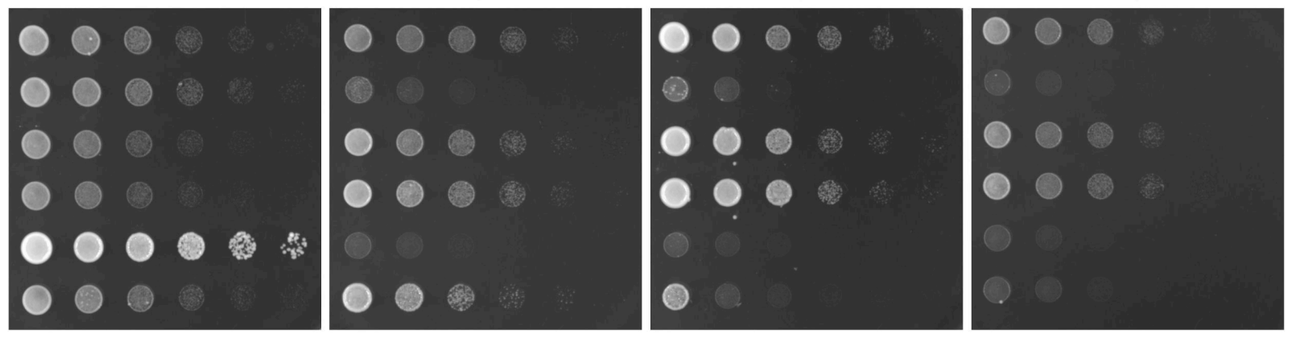

5-Fluorocytosine 40 µM | Fluconazole 150 µM | Ketoconazole 20 µM | Tebuconazole 20 µM

Growth

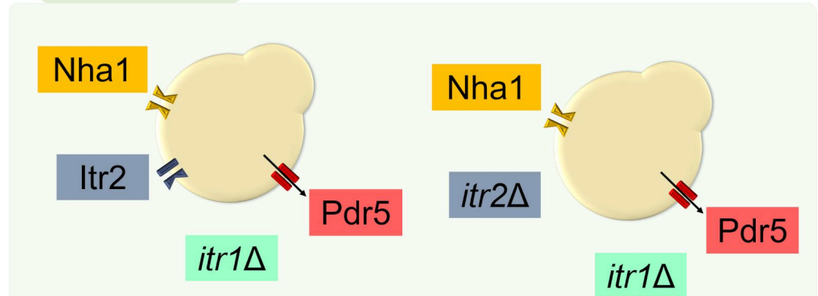

Little growth or death

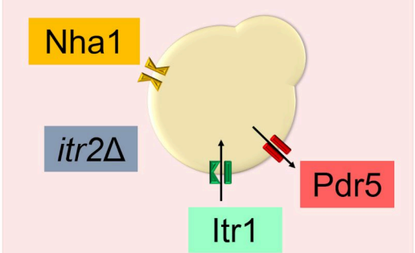

C.

::natMX	::kanMX
itr1Δ	his3Δ
nha1Δ	his3Δ
itr1Δ	nha1Δ
nha1Δ	itr1Δ
fcy2Δ	his3Δ
BY4741	

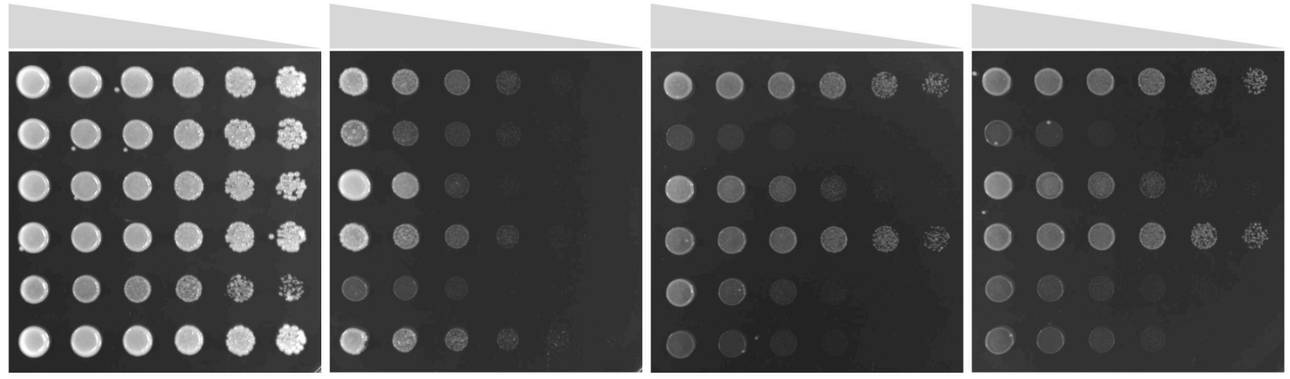

DMSO 1.5 % | Clotrimazole 5 µM | Difenoconazole 4 µM | Epoxiconazole 0.8 µM

itr1Δ	his3Δ
nha1Δ	his3Δ
itr1Δ	nha1Δ
nha1Δ	itr1Δ
fcy2Δ	his3Δ
BY4741	

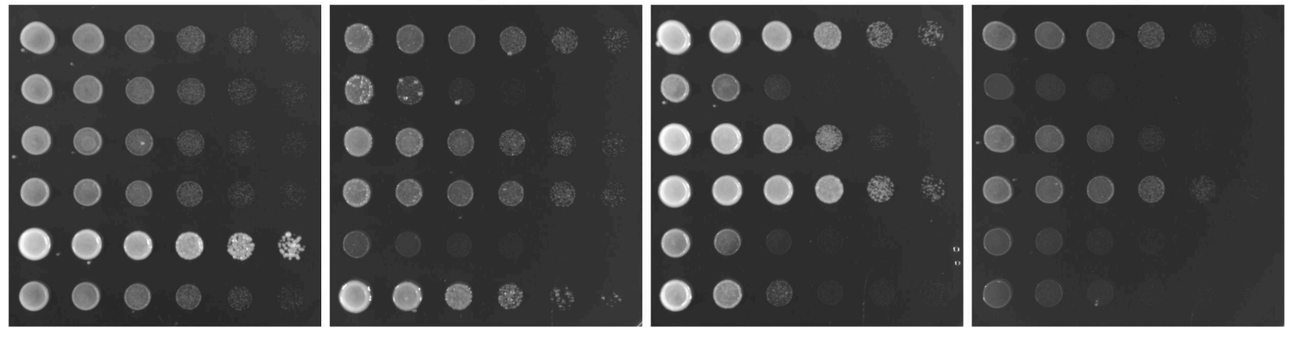

5-Fluorocytosine 40 µM | Fluconazole 150 µM | Ketoconazole 20 µM | Tebuconazole 20 µM

Growth

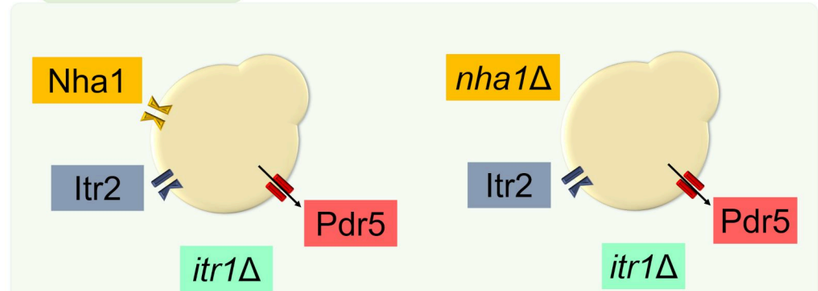

Little growth or death